Geochronology, 4, 121–141, 2022
https://doi.org/10.5194/gchron-4-121-2022


# Late Holocene cryptotephra and a provisional 15 000-year Bayesian age model for Cascade Lake, Alaska

**Lauren J. Davies**[1,2], **Britta J. L. Jensen**[1], **and Darrell S. Kaufman**[3]

[1]Department of Earth and Atmospheric Sciences, University of Alberta, Edmonton, AB, Canada
[2]Department of Geography, University of Cambridge, Cambridge, UK
[3]School of Earth and Sustainability, Northern Arizona University, Flagstaff, Arizona, USA

**Correspondence:** Lauren J. Davies (ld636@cam.ac.uk)

Received: 3 June 2021 – Discussion started: 16 June 2021
Revised: 11 December 2021 – Accepted: 13 January 2022 – Published: 11 March 2022

**Abstract.** Multiple chronometers can be employed for dating Holocene palaeoenvironmental records, each with its own inherent strengths and weaknesses. Radiocarbon dating is one of the most widely used techniques for producing chronologies, but its application at high-latitude sites can sometimes be problematic. Here, cryptotephra were identified in a core from Cascade Lake, Arctic Alaska, and used to identify and resolve an age bias in Late Holocene radiocarbon dates from the top 1.42 m of the sediment sequence. Identifiable geochemical populations of cryptotephra are shown to be present in detectable concentrations in sediment from the north flank of the Brooks Range for the first time. Major-element glass geochemical correlations are demonstrated between ultra-distal cryptotephra and reference samples from the Late Holocene caldera-forming eruption of Opala, Kamchatka, as well as three eruptions in North America: the White River Ash (northern lobe), Ruppert tephra and the Late Holocene caldera-forming eruption of Aniakchak. The correlated ages of these cryptotephra provide evidence for an old-carbon effect and support preliminary palaeomagnetic secular variation (PSV) correlated ages reported for Cascade Lake. Chronological data from Cascade Lake were then combined using a Bayesian approach to generate an age–depth model that extends back through the Late Holocene and provisionally to 15 000 cal yr BP.

## 1 Introduction

The accuracy and precision of ages and chronological models produced from sedimentary records directly impact the utility and value of the associated proxies used for palaeoenvironmental reconstructions. In Arctic North America, the majority of Holocene to Late Pleistocene palaeoenvironmental reconstructions are produced from lake and peat deposits (e.g. Kaufman et al., 2016) and often rely on radiocarbon ($^{14}$C) dating to develop age models.

However, there are several issues that can affect the application and interpretation of $^{14}$C ages in Arctic regions. Firstly, there may be a lack of organic material in lake sediment cores, or the terrestrial macrofossils that are often preferred for dating (e.g. Oswald et al., 2005; Turney et al., 2000) may be absent. This can be a particular problem for sediments that accumulated during colder periods. Secondly, high-latitude regions often have an abundance of old carbon due to slow rates of decomposition in cold, typically nutrient-poor soils (e.g. Gaglioti et al., 2014; Schuur et al., 2008), erosion from the surrounding sediments or bedrock, and the reworking and redeposition of older, well-preserved macrofossils (e.g. Kennedy et al., 2010).

More broadly, $^{14}$C samples can also be affected by issues relating to sample selection, remobilisation, the hard-water effect and contamination (for a general review of these topics see, for example, Olsson, 1974; Lowe and Walker, 2000). These factors can contribute to complicated age models for Arctic sediments that require careful independent verification. For example, the use of bulk sediments for dating has been shown to incorporate organic fractions of varying ages (e.g. Brock et al., 2011; Nelson et al., 1988), and hard-water effects have long been known in North American lakes (e.g. Abbott and Stafford, 1996; Karrow and Anderson, 1975; Moore et al., 1998). It is important to recognise that not all

$^{14}$C ages are affected by these issues, but at Arctic sites their accuracy and reliability cannot be assumed. Additional validation and reassurance provided, for example, by published details of the dated material and the stratigraphic sequences they were extracted from, overlapping independent chronological data, replicate dates, etc., are therefore valuable when attributing confidence to resultant age models.

The combination of multiple chronometers has been successfully used to highlight differences between chronological methods and produce more accurate final age models for lacustrine and peat cores (Davies et al., 2018; Tylmann et al., 2016). Two additional techniques that have been applied in Arctic areas are discussed here – palaeomagnetic secular variation (PSV) and tephrochronology.

### 1.1 Palaeomagnetic chronologies

In recent years there have been an increasing number of studies looking to improve chronologies of late Quaternary Arctic sedimentary sequences by using palaeomagnetic data (e.g. Barletta et al., 2008; Deschamps et al., 2018; Lund et al., 2016; Ólafsdóttir et al., 2013). Sediment records can be sensitive to PSV – small directional changes in the geomagnetic field (Cox, 1970) that are preserved in sediment through the alignment of magnetic mineral grains with Earth's ambient field around the time of deposition. Tie points, identified using peaks and troughs, can then be dated and used as correlative chronostratigraphic tools. These ages can be produced from both individual site measurements and geomagnetic model predictions. PSV correlation techniques are useful as they can produce more frequent data points and be applied beyond the limits of $^{14}$C dating or where organic material is not preserved. Their use, however, is limited geographically as high-latitude geomagnetic field dynamics are spatially complex (e.g. Stoner et al., 2013).

Steen (2016) reports preliminary PSV-correlated ages for cores from Cascade Lake, Alaska, that have substantial offsets during the Late Holocene from $^{14}$C ages from the same sediment. In the upper sections of the core sequence $^{14}$C ages are up to $\sim$ 2000 years older than palaeomagnetic correlated ages. When using multiple chronometers from the same sediment there is not always coherence or clear agreement between the results, as seen here, and additional chronological information is required to produce a reliable age model. In this study tephrochronology was applied to Cascade Lake sediments to investigate this chronological offset.

### 1.2 Cryptotephra chronologies

Cryptotephra – non-visible horizons of volcanic ash from distal sources – have been studied globally (see, e.g., Davies, 2015; Lowe et al., 2017) and are a useful chronostratigraphic tool (Pilcher et al., 1995; Plunkett, 2006; Swindles et al., 2010). Where correlations can be made with well-dated tephra (e.g. historical eruptions or tephra preserved within annually resolved records), tightly constrained associated ages can be included in age–depth models (e.g. Schoning et al., 2005). They can also be used as an independent test of other chronological methods applied to the same record (e.g. Davies et al., 2018; Oldfield et al., 1997).

In Alaska and northern Canada the majority of tephra studies have been limited to areas where visible tephra are present, and only a few studies have discussed cryptotephra (de Fontaine et al., 2007; Lakeman et al., 2008; Monteath et al., 2017; Payne et al., 2008; Zoltai, 1989). However, there is significant potential for cryptotephra to be found in Alaska as it is downwind of a large number of volcanoes known to have been active over the Holocene (Fig. 1; Alaska Volcano Observatory, 2016; Global Volcanism Program, 2013). Of Alaska's 130 volcanoes and volcanic fields, 96 have been active either historically or within the Holocene (Miller et al., 1998), and historical observations show that 54 volcanoes have been active since $\sim$1700 CE alone (Cameron et al., 2020). Here, key tephra are from historical eruptions or eruptions that produced regionally widespread tephra within Alaska and have precise age estimates (Davies et al., 2016).

While there are currently no published occurrences of Kamchatkan tephra within Alaska, the large number of Kamchatkan–Kurile volcanoes active in the Holocene can also be regarded as a potential source of distal cryptotephra, given prevailing wind directions and the large number of recorded major explosive eruptions (e.g. Braitseva et al., 1997; Kyle et al., 2011; Ponomareva et al., 2017). Transcontinental distribution of tephra from non-super eruptions has been established (e.g. Cook et al., 2018; Jensen et al., 2014), and Kamchatkan-sourced tephra has been traced to Greenland, Svalbard and the east coast of North America (van der Bilt et al., 2017; Cook et al., 2018; Jensen et al., 2021; Mackay et al., 2016).

Here, ages from Cascade Lake for cryptotephra and radiocarbon techniques were visually compared and then modelled using Bayesian statistical methods to produce a composite age–depth model. Bayesian techniques have been utilised in a wide range of fields to produce detailed age–depth models based on a relatively small number of dates (e.g. Christen et al., 1995; Litton and Buck, 1995) and, through their inclusion of additional (prior) information, they provide more precise interpolations than using raw dates alone (e.g. Blaauw and Christen, 2005; Bronk Ramsey, 2008).

## 2 Materials and methods

Cascade Lake (68°22′48″ N, 154°36′20″ W; 990 m a.s.l.) lies on the north-central slope of the Brooks Range, the northernmost mountain range in Alaska (Fig. 1). Overall, the Brooks Range is located almost entirely above the Arctic Circle and represents a significant topographic barrier that divides the climatic influences of the Arctic and Pacific oceans. The lake

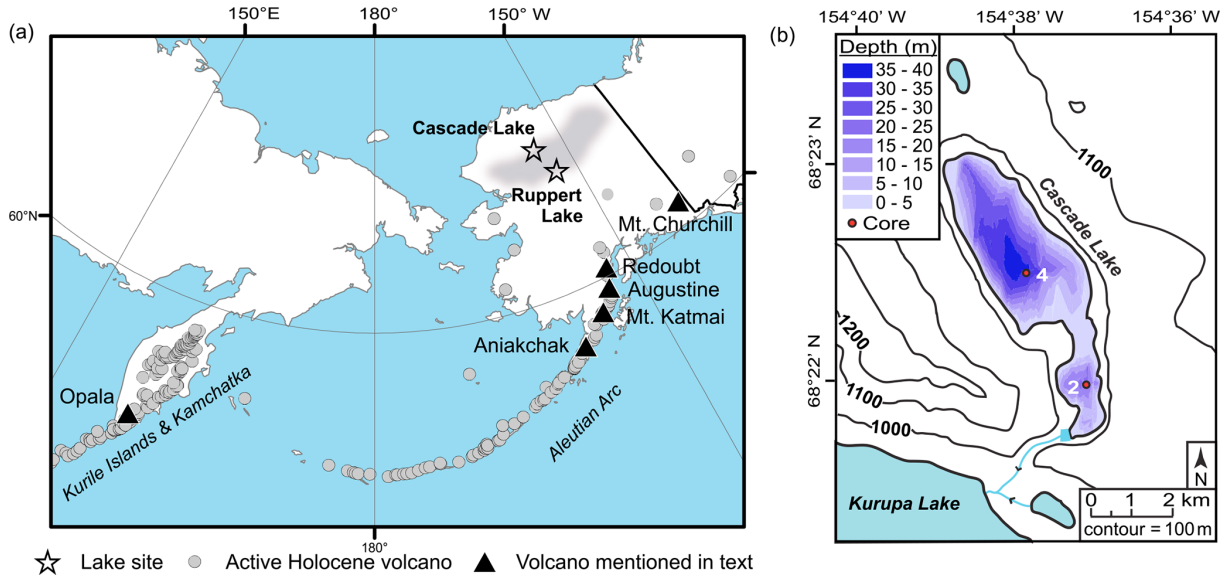


**Figure 1.** Location map showing Cascade Lake, coring sites, and other relevant locations and volcanoes mentioned in the text. Grey circles: active Holocene volcanoes (Global Volcanism Program, 2013); black triangles: volcanic sources mentioned in the text; grey shading: Brooks Range; star outlines: lakes mentioned in the text.

has an area of $\sim 1\,km^2$ and a maximum depth of $\sim 40\,m$ in the main northwestern basin (Fig. 1b) with a total catchment size of $\sim 10\,km^2$. It presently has no significant inflow and one small outflow, west to Kurupa Lake ($\sim 920\,m$ a.s.l.).

In 2013 sediment cores were collected from two sites at Cascade Lake using a percussion-piston coring system (long cores) and an Aquatic Instruments universal corer (surface cores). Cores were split and described at the National Lacustrine Core Facility (LacCore) repository at the University of Minnesota, Twin Cities, and archive halves are housed there. The top 1.42 m of a 5.2 m long composite sedimentary sequence, CASC-4A/2D, is the focus of this study. Analyses were limited to the upper section of the core because (a) it covers the range of depths where a potential offset in ages has been reported (Steen, 2016) and (b) because most well-defined distal tephra deposits in Alaska are limited to the last $\sim 4$ kyr (e.g. Davies et al., 2016).

The CASC-4A/2D sediment cores were undeformed by the coring procedure and the full sequence was separated into three distinct lithologic units based on visual stratigraphy, wet bulk density, organic-matter content and variations in magnetic parameters (Fig. S1 in the Supplement). The new analyses reported here were made from the top 1.42 m of unit 3 (3.55–0 m), which consists of millimetre- to centimetre-scale colour-banded silts and clays. More detailed sediment descriptions are provided by Steen (2016).

## 2.1 Radiometric data

Radiometric data from Cascade Lake (Steen, 2016) are summarised in Table 1. Eleven AMS $^{14}C$ samples analysed at the University of California-Irvine AMS (UCIAMS) Facility are reported. Samples consisted of terrestrial plant macrofossils, insect parts, resting eggs and aquatic vegetation as available. The oldest sample analysed was from 348.5–351 cm and dates to $\sim 15$ ka cal BP. Six $^{210}Pb$ measurements were made from the uppermost sediment at Cascade Lake and equilibrium is reached within the top 4 cm of the sequence (Table 1a; $^{210}Pb$ sediment age of 3–3.5 cm = $143 \pm 7$ years/$1870 \pm 7$ CE).

## 2.2 Cryptotephra detection and analysis

The sampling and analysis of tephra for this study followed best practice guidelines (e.g. Abbott et al., 2021) to facilitate comparability with other research. No visible tephra were located in cores from Cascade Lake; in fact, no visible tephra are known north of the Brooks Range. Targeted cryptotephra analyses were undertaken using contiguous 1 cm thick subsamples from 1.42 m composite depth to the surface. Standard methods (e.g. Blockley et al., 2005) were used to produce glass shard concentration profiles throughout the two core sections. Samples were sieved using 20 µm nylon mesh, and the heavy liquid, lithium heteropolytungstate (LST), was used for density separations.

Glass shard morphologies and grain sizes were recorded using optical microscopy and images of the processed samples (i.e. grains that are $> 20\,\mu m$ and $< 2.45\,g\,cm^{-3}$, mounted in Canada balsam). Shard depths were estimated by recording the number of 3 µm fine-focus increments required to focus through individual grains. Other grain size measurements (e.g. axis lengths, perimeter, maximum pro-

**Table 1.** Radiometric ages produced from Cascade Lake sediment cores (from Steen, 2016): **(a)** $^{210}$Pb ages calculated using the Constant Rate of Supply model (CRS; Appleby and Oldfield, 1978); **(b)** $^{14}$C ages with $\pm$ 1$\sigma$ errors. Ages are reported to the nearest whole year ($^{210}$Pb) or 5 years ($^{14}$C). Italicised rows with sample IDs with [a]: $^{14}$C ages rejected as outliers; [b]: samples from surface core CASC-4B; all other samples are from CASC-4A.

**(a)** $^{210}$Pb CRS ages

| Composite depth (cm) | Age (year) | Error (year) |
|---|---|---|
| 0–0.5 | 23 | 1 |
| 0.5–1 | 48 | 1 |
| 1–1.5 | 67 | 2 |
| 1.5–2.25 | 83 | 2 |
| 2.25–3 | 112 | 4 |
| 3–3.5 | 143 | 7 |

**(b)** $^{14}$C ages

| Composite depth (cm) | Sample ID (UCIAMS no.) | Age ($^{14}$C years) | 1$\sigma$ error ($^{14}$C years) | Material dated |
|---|---|---|---|---|
| 2.6–4.6[b] | 147384 | 170 | 30 | Resting eggs, mixed aquatic fragments |
| *5.5–7.5* | *134422*[a] | *1765* | *20* | Insect remains, twigs, leaves, bryophyte, eggs |
| 11–13[b] | 147383 | 785 | 45 | Leaf fragments, resting eggs, mixed aquatic fragments |
| 30.5–32.5 | 131742 | 2825 | 25 | Insect remains, moss fragments, resting eggs, fine unidentified pieces |
| 85.75–87.75 | 128095 | 4160 | 120 | Insect remains, twigs, leaves, bryophyte, resting eggs |
| 138–140 | 131743 | 5085 | 20 | Insect remains, moss fragments, resting eggs, fine unidentified pieces |
| 197–199 | 131744 | 6485 | 25 | Insect remains, moss fragments, resting eggs, fine unidentified pieces |
| 233.5–235.5 | 134423 | 8270 | 35 | Insect remains, twigs, leaves, resting eggs, fine unidentified pieces |
| *245–248* | *128096*[a] | *13 200* | *450* | Insect remains, aquatic vegetation, twigs, resting eggs |
| 303–304 | 131745 | 9875 | 35 | Insect remains, moss fragments, resting eggs, fine unidentified pieces |
| 348.5–351 | 137726 | 12 690 | 150 | Insect fragments, twig, leaf fragments |

jected area) were calculated using ImageJ software. Values for maximum axis length ($L$) are reported as are geometric size ($d_v$) and sphericity ($\psi$) (calculated following the methods reported in Saxby et al., 2020). As only a small number of measurements were made due to low concentrations of glass present in the sample slides (7–15 shards per sample; Table S1 in the Supplement), these measurements are not fully representative of their source eruptions. For example, Saxby et al. (2020) recommend that 50–500+ measurements are used to characterise mean and maximum shard sizes respectively. However, these quantitative characterisations are reported here as preliminary data for distal deposits of these tephra.

Glass shards for geochemical analysis were re-extracted from peaks in shard concentration using heavy liquid separation. After rinsing, the remaining sample material was pipetted into a pre-drilled hole in an acrylic puck (fixed onto a flat glass plate with double-sided tape) and covered with epoxy resin. Once cured, the flat puck surface was then lightly polished to expose glass surfaces and carbon coated prior to electron probe microanalysis (EPMA). Individual glass shards were analysed on a JEOL 8900 Superprobe at the University of Alberta by wavelength dispersive X-ray spectroscopy (WDS) following established protocols (e.g. Jensen et al., 2008, 2019).

A standard suite of 10 elements (Si, Ti, Al, Fe, Mn, Mg, Ca, Na, K, Cl; 30 s peak count times; ZAF correction method) was measured using a 5 µm beam with 15 keV accelerating voltage and 6 nA beam current. This focussed beam (usually 10 µm is utilised) can result in Na loss in more sensitive glasses. However, where intensity data loss does occur, it has been shown that empirical corrections can be applied if the data demonstrate linear variance over time (Nielsen and Sigurdsson, 1981). Here Na, and if necessary, Si, were corrected for time-dependent intensity (TDI) loss (or gain) using a self-calibrated correction with the Probe for EPMA software (Donovan et al., 2015). This method at these settings has been successfully applied in several studies on tephra of different compositions and grain sizes (Foo et al., 2020; Jensen et al., 2019, 2021).

Two secondary standards of known composition were run concurrently with all tephra samples: ID 3506, a Lipari rhyolite obsidian, and a reference sample of Old Crow tephra, a well-characterised, secondarily hydrated tephra bed (Kuehn et al., 2011). All results were normalised to 100 % and are presented as weight percent (wt %) oxides. New major-

element geochemical data and associated standard measurements, as well as data points for relevant reference material (analysed concurrently, where possible), are reported in the Supplement (Tables S2–S4). Non-glass analyses (e.g. minerals, biogenic silica) and analyses with analytical totals $< 94$ % were rejected but are still shown in Tables S2 and S3.

Correlations to known tephra or volcanic sources were based on major-element geochemistry (including concurrent re-analyses with reference materials where possible), stratigraphic position and consistent glass morphological characteristics.

### 2.3 Bayesian age modelling

Three steps are detailed here for identifying and resolving problematic chronometer offsets using the radiometric data from Steen (2016) and new cryptotephra-correlated ages. Both manual approaches and statistical outlier analysis techniques included in OxCal v4.4 (Bronk Ramsey, 2009a, b) are applied in the following order.

Firstly, ages that were obviously out of stratigraphic sequence (previously highlighted by Steen, 2016) were rejected. Secondly, OxCal's Poisson process model (P_Sequence, Bronk Ramsey, 2008) was used to construct independent models for each chronometer. IntCal20 (Reimer et al., 2020) and Bomb21NH1 (Hua et al., 2021) were used for $^{14}$C calibrations as appropriate. The independent models were visually compared to detect offsets between the dating methods, and outliers were identified statistically using OxCal's agreement indices (AI), which show the extent to which the modelled posterior distributions overlap with the original distributions. Here, $^{210}$Pb dates from 0–3.5 cm are used to check for agreement with the uppermost $^{14}$C age (2.6–4.6 cm) and cryptotephra isochrons are used as independent checks on the remaining Late Holocene $^{14}$C ages. Comparing separate independent models is an effective preliminary check of the data, especially where there is an imbalance between the number and the resolution of dates used from each chronometer, which may bias statistical outlier analysis techniques. For example, this is demonstrated by the assessment of $^{210}$Pb and $^{14}$C ages from peatbogs in Alberta, Canada, reported in Davies et al. (2018).

Finally, the remaining chronological data were combined in one composite P_Sequence model (OxCal v4.4; Bronk Ramsey, 2009a). This set-up allows variable accumulation rates; here the $k$ parameter (deposition events defined as increments per unit length, controlling model rigidity and resolution) was set as variable rather than fixed to increase model flexibility (Bronk Ramsey and Lee, 2013). At this stage, general (Student's $t$) outlier analysis was used to identify any remaining anomalous ages in the parsed dataset (Bronk Ramsey, 2009b). All ages were given the prior probability of 5 % of ages being incorrect; if an age needed to be shifted substantially (by more than 2 standard deviations) to fit the resulting age–depth model, it was identified as an outlier and downweighed in the process (Blockley et al., 2007).

## 3 Cryptotephra abundance and geochemical data

Glass shards were present in $\sim 75$ % of the samples analysed in this study (108 out of 143 total samples). The composite shard concentration profile for the 1.42 m of core samples analysed here is shown in Fig. 2. Twenty-eight peaks were chosen for geochemical analysis based on the relative abundances of shards counted at those depths. This generally was around 4–42 shards g$^{-1}$, except for the top 0–1 cm, which had 88 shards g$^{-1}$. For each sample, geochemical analyses were performed on single grains, but 15 of the peaks chosen resulted in fewer than five shards exposed on the EPMA puck surface. This is likely due to the relatively low concentrations of glass present overall.

Of the remaining 13 samples, 5 have dominant unique geochemical populations (i.e. primary deposits, likely relating to a single eruption, are strongly represented), 6 have multiple identifiable trends and/or populations (representing an amalgamation of shards from multiple eruptions), and 2 have sparse shards with no discernible geochemical trends. Table 2 and Fig. 3 show the samples analysed, the average major-element data for identified geochemical populations, and any geochemical correlations to known eruptions with associated chronological data or similarities to known volcanic sources. Normalised single-point major-element geochemical data (Table S2), associated standard analyses (Table S3) and all unnormalised data (Table S4) are provided in the Supplement.

The shard abundance profile shows multiple closely spaced peaks and tails (Fig. 2) that translate into several samples containing multimodal geochemical populations, especially in the top 30 cm of the core. This could be evidence for taphonomic problems (e.g. reworking, bioturbation), but a lack of evidence for sediment reworking and an abundance of eruptions in the Late Holocene suggest this is not a substantial problem at Cascade Lake (see the "Multimodal samples and historical activity" section below for detailed discussion).

### 3.1 Unique glass populations

Five of the analysed samples contained glass shards that show dominant unimodal rhyolitic geochemical populations based on between 10 and 36 individual point analyses. These are interpreted as primary tephra-fall events relating to contemporaneous eruptions. Grain size data were measured for 7 to 15 shards per sample and show that average maximum axis length and sphericity values are very similar for all five samples ($L = 23$–$27$ µm and $\psi = 0.56$–$0.63$ respectively). Four of these five samples can be used as isochrons as they correlate to reference material from known and dated eruptions (University of Alberta reference collection samples, Fig. 3;

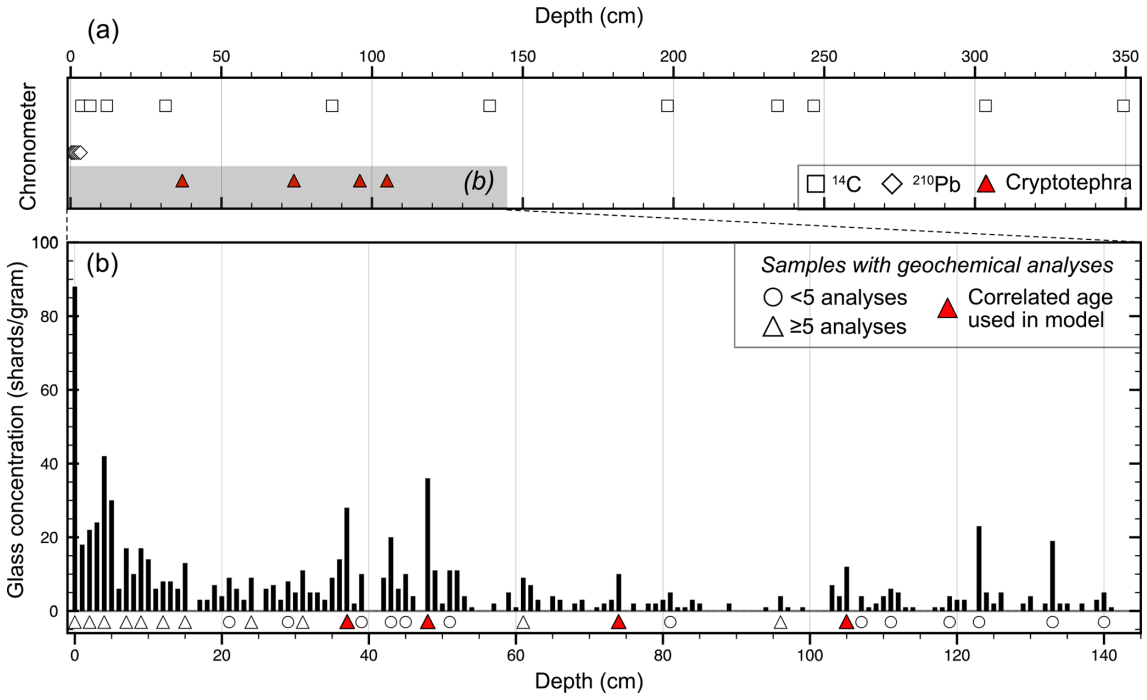


**Figure 2.** Cascade Lake core CASC-4A/2D chronological controls. **(a)** The composite depths of radiometric ages ($^{14}$C and $^{210}$Pb; Table 1) and correlated cryptotephra ages (Tables 2a and 3). The shaded grey area shows the depth interval of core sampled for cryptotephra analysis (expanded in panel **b**). **(b)** Glass shard concentration counts produced down to 1.42 m, and the composite depths of analysed glass peaks. Geochemical analysis was carried out for 28 of the 142 samples: circles: $< 5$ points analysed; triangles: $> 5$ points analysed; filled red triangles have correlated ages that are used in the age–depth model.

details provided in Tables 2 and S2). Key information regarding these eruptions and the tephra deposits are summarised in Table 3. Grain size data and shard images are presented in the Supplement (Table S1 and Fig. S2). Samples are discussed here individually from oldest to youngest and previously published age estimates are given as $2\sigma$ $^{14}$C calibrated age ranges unless otherwise stated.

### 3.1.1 CL-105 (Aniakchak Caldera Forming Eruption, CFE, II)

CL-105, a peak concentration of 12 shards g$^{-1}$, is characterised by platy and cuspate shards. It is a geochemical match for the dominant rhyodacite population of the widespread Late Holocene caldera-forming eruption of Aniakchak (CFE II) (Fig. 3; see Bacon et al., 2014; Neal et al., 2001; Riehle et al., 1987, for details). Tephra from this eruption has been found visibly across southern and western Alaska and as cryptotephra in the Bering Sea, Yukon, Newfoundland and Greenland (Davies, 2018; Denton and Pearce, 2008; Pearce et al., 2017, 2004; Ponomareva et al., 2018; Pyne-O'Donnell et al., 2012). A small second population of four points was also identified in this sample (CL-105b, Table 2c); they do not correlate with reference material for this eruption (e.g. Wallace et al., 2017), but it is unclear if these represent a separate event or shards from the main population with alkali loss.

Chronologically, the Aniakchak CFE II tephra has disparate age estimates where modelled radiocarbon dates and ice core ages are notably offset (see Davies et al., 2016, for a detailed summary of references). Radiocarbon age estimates have been produced from sequences with visible tephra as well as distal lakes and peat bogs with correlated cryptotephra. A precise ice core model age estimate is associated with distal cryptotephra identified in North Greenland Ice Core Project (NGRIP) samples.

The identification of an eruption event in NGRIP is supported using geochemically correlated glass shards and sulfate peaks (Coulter et al., 2012; Pearce et al., 2004). Additional evidence for the eruption is also provided by tree ring perturbations during this interval (Baillie and McAneney, 2015), which have been correlated to the NGRIP records. Geochemically correlated glass shards in two NGRIP intervals have overlapping GICC05 modelled ages of 3594–3589 BP (1641–1639 BCE – QUB-1198, 1644–1643 BCE – QUB 1201; Coulter et al., 2012; Vinther et al., 2006). Differences in the IntCal13 and GICC05 timescales over the Holocene were quantified by a transfer function developed by Adolphi and Muscheler (2016), using common variations in $^{14}$C and $^{10}$Be production rates (recorded in tree rings and ice cores respectively). If their correction factor for this time

**Table 2.** Normalised average major-element geochemical glass data for identifiable populations of analysed tephra samples and suggested correlations. Popn: unimodal geochemical data are labelled as "–"; where multiple geochemical populations are identified, they are labelled separately (e.g. a, b), but if they are interpreted as being related heterogenous populations a combined average is also shown (e.g. a+b). $FeO_t$: total iron oxide as FeO; $H_2O_d$: water by difference; numbers listed in brackets: 1 SD. **(a)** Main populations. **(b)** Reference material analysed at the University of Alberta; for full details regarding the original sample details please see listed references. **(c)** Samples with multiple populations or too few points to use as tie points. Only groups of three or more analyses are shown here – for full details see Table S2.

**(a)** Main populations

| Sample no. | Popn | $SiO_2$ | $TiO_2$ | $Al_2O_3$ | $FeO_t$ | MnO | MgO | CaO | $Na_2O$ | $K_2O$ | Cl | $H_2O_d$ | *n* | Correlation |
|---|---|---|---|---|---|---|---|---|---|---|---|---|---|---|
| CL-37 | – | 76.73 (0.26) | 0.11 (0.03) | 13.27 (0.12) | 0.60 (0.09) | 0.08 (0.03) | 0.12 (0.02) | 0.77 (0.04) | 4.39 (0.23) | 3.83 (0.22) | 0.12 (0.02) | 3.90 (1.31) | 10 | Opala (OP) |
| CL-48 | a | 74.52 (0.58) | 0.22 (0.06) | 14.12 (0.32) | 1.49 (0.20) | 0.06 (0.01) | 0.34 (0.08) | 1.57 (0.13) | 4.07 (0.27) | 3.35 (0.25) | 0.34 (0.03) | 2.23 (1.58) | 10 | Mt Churchill – White River Ash |
| | b | 77.76 (0.69) | 0.16 (0.05) | 12.43 (0.42) | 1.06 (0.10) | 0.04 (0.02) | 0.15 (0.04) | 0.91 (0.18) | 3.65 (0.16) | 3.61 (0.19) | 0.30 (0.04) | 2.25 (1.89) | 12 | (northern lobe, WRAn) |
| | a+b | 76.29 (1.77) | 0.19 (0.06) | 13.20 (0.94) | 1.26 (0.26) | 0.05 (0.02) | 0.24 (0.11) | 1.21 (0.37) | 3.84 (0.30) | 3.49 (0.25) | 0.31 (0.04) | 2.24 (1.71) | 22 | |
| CL-74 | – | 74.16 (0.63) | 0.30 (0.05) | 13.91 (0.23) | 1.96 (0.15) | 0.11 (0.02) | 0.46 (0.06) | 2.18 (0.14) | 4.81 (0.26) | 1.91 (0.09) | 0.25 (0.03) | 0.48 (1.24) | 36 | Ruppert |
| CL-96 | – | 74.04 (0.95) | 0.40 (0.03) | 13.72 (0.46) | 1.89 (0.15) | 0.08 (0.02) | 0.49 (0.09) | 2.06 (0.18) | 4.33 (0.23) | 2.81 (0.08) | 0.24 (0.02) | 0.86 (1.18) | 12 | unknown |
| CL-105 | a | 71.10 (0.29) | 0.48 (0.03) | 15.19 (0.15) | 2.34 (0.07) | 0.13 (0.02) | 0.52 (0.03) | 1.64 (0.04) | 5.53 (0.23) | 2.91 (0.12) | 0.20 (0.02) | 0.54 (0.93) | 11 | Aniakchak CFE II |

**(b)** Reference material analyses from the University of Alberta

| Site | Sample ID | $SiO_2$ | $TiO_2$ | $Al_2O_3$ | $FeO_t$ | MnO | MgO | CaO | $Na_2O$ | $K_2O$ | Cl | $H_2O_d$ | *n* | Correlation | Reference sample details |
|---|---|---|---|---|---|---|---|---|---|---|---|---|---|---|---|
| Duke River Fan, YT | UA 1044 | 74.32 (0.63) | 0.21 (0.05) | 14.18 (0.33) | 1.54 (0.15) | 0.06 (0.03) | 0.32 (0.05) | 1.67 (0.16) | 4.11 (0.18) | 3.26 (0.13) | 0.33 (0.04) | 2.40 (1.15) | 55 | White River Ash (northern lobe) | Jensen (2007) |
| Sixtymile River | UT 1480, Sample 16 | 73.95 (2.06) | 0.21 (0.07) | 14.38 (0.99) | 1.50 (0.31) | 0.06 (0.03) | 0.35 (0.14) | 1.77 (0.49) | 4.29 (0.31) | 3.23 (0.19) | 0.34 (0.04) | 2.82 (0.78) | 31 | White River Ash | Preece et al. (2014), |
| area, YT | UT 1482, Sample 17 | 73.65 (1.80) | 0.23 (0.06) | 14.50 (0.87) | 1.59 (0.29) | 0.06 (0.02) | 0.38 (0.12) | 1.83 (0.46) | 4.26 (0.26) | 3.25 (0.19) | 0.34 (0.05) | 3.06 (0.88) | 34 | (northern lobe) | this paper |
| Zagoskin Lake, | UA 1602a, | 59.13 (0.97) | 1.40 (0.07) | 16.45 (0.16) | 7.50 (0.64) | 0.22 (0.03) | 2.97 (0.22) | 6.06 (0.40) | 4.61 (0.26) | 1.57 (0.11) | 0.13 (0.02) | 2.30 (1.07) | 17 | Aniakchak CFE II | Ager (2003), |
| AK | UA 1602b | 71.07 (0.52) | 0.50 (0.05) | 15.19 (0.28) | 2.55 (0.20) | 0.14 (0.03) | 0.51 (0.08) | 1.78 (0.19) | 5.07 (0.29) | 3.05 (0.13) | 0.19 (0.02) | 2.48 (1.56) | 32 | (andesite, rhyodacite) | Davies et al. (2016) |
| Ruppert Lake, AK | UA 2557 | 74.08 (0.39) | 0.30 (0.05) | 13.96 (0.16) | 2.00 (0.12) | 0.10 (0.03) | 0.46 (0.04) | 2.18 (0.10) | 4.80 (0.14) | 1.93 (0.10) | 0.22 (0.02) | 0.53 (0.90) | 17 | Ruppert | Monteath et al. (2017) |
| Southern Kamchatka | UA 3286, OP-22-U | 76.65 (0.20) | 0.12 (0.04) | 13.31 (0.12) | 0.69 (0.03) | 0.11 (0.03) | 0.12 (0.02) | 0.77 (0.03) | 4.24 (0.11) | 3.91 (0.09) | 0.11 (0.02) | 2.65 (0.71) | 30 | Opala (Phase III) | Andrews et al. (2018) |

interval ($-19 \pm 3$ years) is applied to the GICC05 chronology, the resulting NGRIP modelled age for the eruption is $3572 \pm 4$ cal yr BP (1 SD; Adolphi and Muscheler, 2016; Pearce et al., 2017).

Here we report updated modelled eruption ages produced using the Tau_Boundary function in OxCal v.4.4 (Bronk Ramsey, 2009a) with IntCal20 (Reimer et al., 2020) following Davies et al. (2016; Fig. S3 of this paper, see Table S5 for details). The Tau_Boundary function is used here for both the upper and lower boundaries around a single-phase eruptive event. All dates associated with the tephra are included in the model, with an exponential rise and fall before and after the eruption event (i.e. assuming that dates cluster closely around the event). For Aniakchak CFE II, the ice core modelled age discussed above is only compatible with published $^{14}C$ ages if two of the three $^{14}C$ ages that underlie the tephra in an exposed peat section in northwest Alaska (Blackford et al., 2014) are removed as outliers. This is unexpected because the peat section is one of the most precisely dated terrestrial sequences for Aniakchak CFE II, with six samples analysed at 0.5 cm increments over 3 cm immediately surrounding the tephra. While there are no obvious reasons for disregarding these two ages, beyond the disagreement with the ages from the ice cores, in this instance it seems pertinent

**Table 2.** Continued.

| **(c)** Other samples analysed | | | | | | | | | | | | | |
|---|---|---|---|---|---|---|---|---|---|---|---|---|---|
| Sample | Popn | $SiO_2$ | $TiO_2$ | $Al_2O_3$ | $FeO_t$ | MnO | MgO | CaO | $Na_2O$ | $K_2O$ | Cl | $H_2O_d$ | *n* |
| CL-0 | a | 71.02 (0.29) | 0.48 (0.03) | 14.90 (0.15) | 2.36 (0.08) | 0.16 (0.03) | 0.50 (0.02) | 1.67 (0.05) | 5.64 (0.26) | 3.09 (0.08) | 0.23 (0.03) | 1.46 (1.26) | 7 |
| | b | 74.42 (1.46) | 0.16 (0.04) | 13.99 (0.76) | 1.28 (0.28) | 0.05 (0.02) | 0.32 (0.12) | 1.57 (0.29) | 4.63 (0.13) | 3.33 (0.12) | 0.33 (0.01) | 3.12 (1.59) | 3 |
| | c | 74.68 (0.84) | 0.32 (0.04) | 13.68 (0.67) | 2.02 (0.16) | 0.09 (0.02) | 0.46 (0.04) | 2.22 (0.19) | 4.43 (0.34) | 1.94 (0.05) | 0.21 (0.06) | 1.78 (0.62) | 6 |
| | d | 75.63 (1.35) | 0.26 (0.10) | 13.51 (0.44) | 1.22 (0.41) | 0.05 (0.01) | 0.31 (0.10) | 1.30 (0.38) | 4.54 (0.45) | 3.05 (0.19) | 0.15 (0.07) | 2.32 (1.05) | 6 |
| | e | 76.91 (0.45) | 0.33 (0.04) | 12.27 (0.09) | 1.57 (0.11) | 0.03 (0.01) | 0.26 (0.02) | 1.16 (0.02) | 4.33 (0.33) | 2.97 (0.01) | 0.21 (0.01) | 1.61 (0.48) | 3 |
| CL-2 | a | 71.00 (0.59) | 0.49 (0.10) | 15.00 (0.23) | 2.48 (0.34) | 0.14 (0.03) | 0.52 (0.10) | 1.68 (0.20) | 5.42 (0.16) | 3.11 (0.14) | 0.22 (0.03) | 1.35 (0.78) | 14 |
| | b | 73.73 (0.35) | 0.21 (0.02) | 14.46 (0.23) | 1.51 (0.05) | 0.04 (0.03) | 0.37 (0.03) | 1.77 (0.10) | 4.52 (0.12) | 3.13 (0.08) | 0.33 (0.02) | 2.81 (1.14) | 5 |
| | c | 74.17 (0.45) | 0.32 (0.03) | 13.75 (0.16) | 1.94 (0.08) | 0.12 (0.02) | 0.45 (0.01) | 2.20 (0.18) | 4.82 (0.23) | 2.03 (0.04) | 0.26 (0.01) | 1.14 (0.74) | 4 |
| | d | 75.86 (0.27) | 0.25 (0.04) | 13.18 (0.14) | 1.56 (0.05) | 0.07 (0.03) | 0.31 (0.04) | 1.66 (0.11) | 4.96 (0.14) | 2.01 (0.03) | 0.17 (0.02) | 2.04 (0.28) | 4 |
| | e | 76.90 (1.24) | 0.26 (0.16) | 12.63 (0.35) | 1.19 (0.52) | 0.07 (0.02) | 0.22 (0.12) | 1.05 (0.38) | 4.20 (0.23) | 3.35 (0.34) | 0.18 (0.11) | 3.07 (0.93) | 5 |
| CL-4 | a | 66.61 (1.64) | 0.77 (0.26) | 15.68 (0.22) | 4.45 (1.07) | 0.13 (0.05) | 1.19 (0.14) | 3.50 (0.44) | 4.88 (0.3) | 2.63 (0.12) | 0.20 (0.11) | 1.79 (0.79) | 4 |
| | b | 70.86 (0.86) | 0.49 (0.04) | 15.00 (0.17) | 2.47 (0.35) | 0.14 (0.03) | 0.51 (0.08) | 1.69 (0.18) | 5.50 (0.36) | 3.17 (0.3) | 0.22 (0.02) | 1.09 (0.91) | 15 |
| | c | 76.71 (0.16) | 0.12 (0.04) | 13.26 (0.02) | 0.61 (0.17) | 0.12 (0.03) | 0.09 (0.06) | 0.72 (0.03) | 4.25 (0.18) | 4.07 (0.36) | 0.10 (0.04) | 2.78 (0.86) | 3 |
| CL-7 | a | 70.93 (0.19) | 0.48 (0.02) | 15.03 (0.12) | 2.36 (0.09) | 0.13 (0.04) | 0.59 (0.13) | 1.88 (0.38) | 5.40 (0.45) | 3.03 (0.20) | 0.20 (0.03) | 1.04 (0.15) | 5 |
| | b | 75.83 (0.61) | 0.23 (0.05) | 13.31 (0.39) | 1.55 (0.04) | 0.07 (0.03) | 0.33 (0.08) | 1.67 (0.24) | 4.82 (0.23) | 2.06 (0.1) | 0.16 (0.04) | 1.63 (0.62) | 6 |
| CL-31 | | 77.92 (0.7) | 0.13 (0.02) | 12.22 (0.55) | 1.06 (0.1) | 0.06 (0.03) | 0.15 (0.04) | 0.85 (0.23) | 3.84 (0.34) | 3.53 (0.26) | 0.31 (0.01) | 1.97 (1.16) | 6 |
| CL-61 | a | 71.23 (0.80) | 0.43 (0.04) | 15.05 (0.28) | 2.39 (0.07) | 0.15 (0.02) | 0.44 (0.05) | 1.57 (0.13) | 5.50 (0.56) | 3.09 (0.19) | 0.20 (0.02) | -0.28 (0.28) | 3 |
| | b | 77.70 (0.33) | 0.21 (0.02) | 12.72 (0.20) | 1.23 (0.07) | 0.05 (0.03) | 0.34 (0.01) | 2.05 (0.05) | 4.01 (0.16) | 1.62 (0.09) | 0.10 (0.02) | 0.44 (1.40) | 4 |
| CL-105 | b | 71.81 (0.55) | 0.51 (0.09) | 14.75 (0.03) | 2.32 (0.22) | 0.10 (0.02) | 0.41 (0.05) | 1.43 (0.13) | 4.85 (0.22) | 3.69 (0.04) | 0.17 (0.01) | 0.37 (0.14) | 4 |

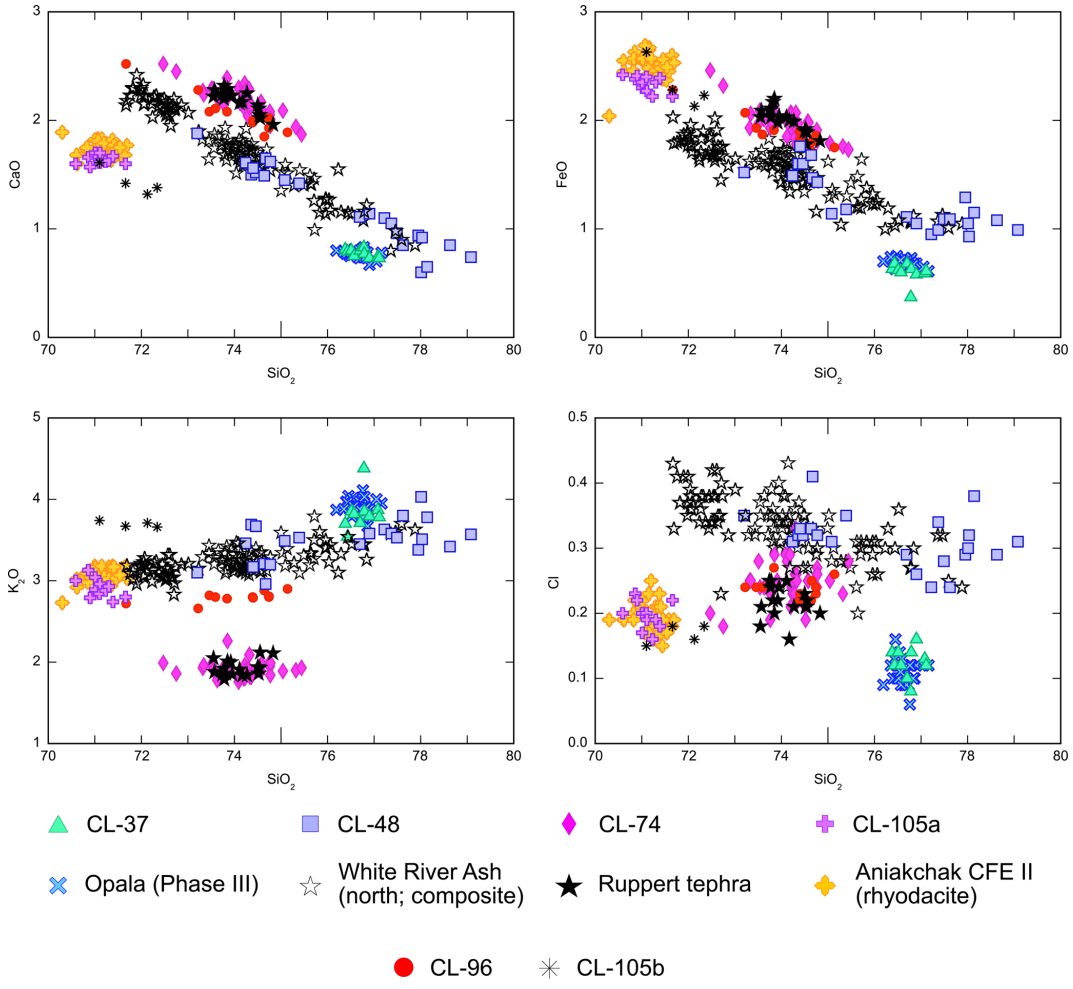


**Figure 3.** Geochemical biplots showing major-element data for the five unique populations of cryptotephra glass identified from Cascade Lake sediment and data for reference material where relevant. Points for CL-105b are also plotted, for reference. See Table 2 for sample details and Table S2 for individual point data.

to do so. Modelled Tau_Boundary estimates for the eruption age are (a) 3545–3425 cal yr BP when all $^{14}$C dates are included, (b) 3610–3450 cal yr BP with two $^{14}$C dates removed, and (c) 3590–3545 cal yr BP including all but two $^{14}$C dates and the NGRIP ice core chronology age (Fig. S3). At Cascade Lake, using either the ice core chronology age estimate of $3572 \pm 4$ cal yr BP (Adolphi and Muscheler, 2016; Pearce et al., 2017) or the Tau_Boundary model age (c, above) for Aniakchak CFE II shows that this age is younger than the radiometric age-model estimate for this depth by $\sim$ 1000–1800 years (Table S6).

### 3.1.2 CL-96 (unknown)

CL-96 represents a small peak of only 4 shards g$^{-1}$, but analytical points were obtained from 10 individual shards. These data show relatively high values for wt % $TiO_2$, $FeO_t$ and CaO (Table 2a) and are similar to CL-74 for many major elements but have substantially higher wt % $K_2O$ (2.81 wt % average vs. 1.91 wt % respectively). The shards are likely from a source in Alaska and the Aleutian Arc and are similar to published average analyses for glass from the Katmai volcanic cluster (Fierstein, 2007) but cannot be directly correlated here to a particular vent or eruption. Therefore, there are no associated age estimates that can be used here to compare with other Cascade Lake chronometers. For future comparisons, the few observed shards from CL-96 were typically chunky with a small number of vesicles or cuspate edges and the final age-model estimate for this depth is 3550–2920 cal yr BP ($2\sigma$; Table S7).

### 3.1.3 CL-74 (Ruppert tephra)

CL-74 has a shard concentration peak of 10 shards g$^{-1}$ but a disproportionately high number of analyses (38) when compared to other samples. This rhyolitic glass population of platy and cuspate shards has relatively low wt % $K_2O$ values ($\sim$ 2.0 %) compared to most other known tephra from

**Table 3.** Cascade Lake cryptotephra and its suggested correlative eruptions. Radiocarbon modelled age estimates produced in this paper for the core depth of the cryptotephra are compared with published ages for the listed eruptions. Bayesian modelled ages for both Aniakchak CFE II and Opala are updated here using OxCal v4.4 (Bronk Ramsey, 2009a) and IntCal20 (Reimer et al., 2020).

| Sample (lab no.) | Suggested correlation | | Cascade Lake | Age estimate for correlated eruption | | | |
|---|---|---|---|---|---|---|---|
| | Tephra | Source volcano | $^{14}$C age (cal yr BP) | 95 % range (cal yr BP) | Method | Deposit type | Age estimate reference(s) |
| CL-37 (UA 3721) | OP | Opala, Kamchatka | 3300 to 2800 | 1395 to 1305 | Calibrated $^{14}$C (IntCal20) | Visible tephra (Kamchatka) | Braitseva et al. (1995); updated here using IntCal20 |
| CL-48 (UA 3730) | WRAn | Mt Churchill, Alaska | 3780 to 2980 | 1689 to 1540 | Calibrated $^{14}$C (IntCal20) | Visible tephra (Alaska, Yukon) | Reuther et al. (2020) |
| CL-74 (UA 3733) | Ruppert | Unknown (likely Alaska) | 4595 to 3700 | 2800 to 2130 | Calibrated $^{14}$C (IntCal20) | Distal cryptotephra (four bogs – Newfoundland, Canada; Maine, Michigan, New York, USA) | Jensen et al. (2021) |
| CL-96 (UA 3735) | – | Unknown | 5130 to 4380 | – | – | – | – |
| CL-105a (UA 3736) | CFE II | Aniakchak, Alaska | 5375 to 4575 | 3590 to 3545 | Calibrated $^{14}$C (IntCal20) and ice core | Visible tephra (Alaska) and cryptotephra (Alaska, USA; Newfoundland, Canada) | Davies et al. (2016); updated here using IntCal20 |
| | | | | $3572 \pm 8$ ($-19 \pm 3$) | GICC05 (with correction) | Distal cryptotephra (North Greenland Ice Core Project, NGRIP, Greenland) | Vinther et al. (2006); Adolphi and Muscheler (2016); Pearce et al. (2017) |

Alaska and is a geochemical match for the Ruppert tephra. This tephra was first identified in Newfoundland (NDN-230; Pyne-O'Donnell et al., 2012) and tentatively correlated to Augustine G tephra, although this is now known to be incorrect (Blockley et al., 2015; Monteath et al., 2017). While it is geochemically similar to glass from Augustine volcano, no proximal correlative is currently known. The tephra was later found in, and subsequently named after, Ruppert Lake, directly south of Cascade Lake on the southern slope of the Brooks Range (Monteath et al., 2017) and has also been identified in peatlands in the Yukon (Davies, 2018) and eastern USA (Jensen et al., 2021).

It is an unusual situation to have a distal tephra deposit correlated between multiple sites that are located up to 5000 km apart but with no identified visible deposits. Such a correlation relies heavily on the geochemical characterisation and coincident timing. While there was some uncertainty about the validity of the geochemical correlation between sites from previously published data that were analysed at different times, this has recently been addressed with concurrently analysed samples from Alaska and the eastern USA and Canada by Jensen et al. (2021). Regardless of where Ruppert tephra is sourced from, we are confident in this correlation to Cascade Lake, as Ruppert tephra has been reported (and named) in this region and its presence in Alaska is firmly established.

Chronologically, the $^{14}$C age models from Ruppert Lake, Alaska, show some evidence of old carbon contamination (core RS: 3230–2930 cal yr BP; core RC: 2920–2520 cal yr BP; Monteath et al., 2017), and these are therefore not interpreted as accurate for constraining the eruption age. Instead, our recommended best age estimate is a modelled $^{14}$C age of 2800–2130 cal yr BP ($2\sigma$; Jensen et al., 2021) produced from distal deposits in four peat bogs (located in Newfoundland, Canada; Maine, Michigan and New York, USA). This age is younger than the radiometric age-model estimate for this depth at Cascade Lake by $\sim$ 1240–2130 years (Table S6).

#### 3.1.4 CL-48 (White River Ash, northern lobe)

CL-48 is the largest glass concentration peak of the pre-19th-century sequence, with 36 shards $g^{-1}$. These vesicular to frothy rhyolitic glass shards typically contain large numbers of microlite inclusions. They are geochemically similar to the White River Ash, which comprises two Late Holocene eruptions from Mt Churchill (Lerbekmo, 2008; Preece et al., 2014). Major-element glass geochemical data for these eruptions are very similar (with substantial overlap), but given the geographic relationship to the main plume directions, broad range of wt % $SiO_2$ values and bimodal geochemistry of CL-48 shards, CL-48 likely correlates with the older northern-focused eruption (WRAn). The tephra from this eruption is more geochemically diverse than that of the younger eastern lobe (Davies et al., 2019) and is preserved as a visible bed in sediment deposits north of the vent in Alaska and the Yukon.

Reference geochemical data from three WRAn samples in the Yukon (Jensen, 2007; Preece et al., 2014) are plotted in Fig. 3 to demonstrate the observed variability; distal correlatives trend towards higher wt % $SiO_2$ values compared to proximal samples. While geochemical differences between sites may tend to preclude a correlation, available analyses show that distal WRAn does vary geochemically by geographic location, although the entire geochemical trend is present more proximal to the volcano. Whether this is the result of a layered magma chamber or multiple, closely spaced eruptions, is unclear (e.g. Preece et al., 2014). Regardless, this manifests with the most distal cryptotephra samples trending towards having the highest average $SiO_2$ values, which is reflected in the Cascade Lake sample (e.g. Davies et al., 2019; Harvey, 2021).

WRAn has a recently updated modelled $2\sigma$ $^{14}C$ age of 1689–1560 cal yr BP (Reuther et al., 2020). This is slightly younger than previous published estimates (e.g. 1805–1605 cal yr BP, Davies et al., 2016) as the eruption occurred at a time when there is a fluctuation in the $^{14}C$ calibration curve. An increased number of constraining ages can therefore adjust the most likely modelled age. At Cascade Lake, this age is younger than the radiometric age-model estimate for this depth by ∼ 1370–2170 years (Table S6).

#### 3.1.5 CL-37 (OP tephra)

CL-37 is the second largest pre-19th-century peak, with 28 shards $g^{-1}$. Shards are typically vesicular or cuspate and often have microlite inclusions. This rhyolitic glass population is distinctive from published analyses of glass from Alaska, with notably low wt % $FeO_t$ (average 0.60 %) and CaO (average 0.77 %). This characteristic geochemical signature has been observed in some volcanic glasses from Kamchatka (e.g. Portnyagin et al., 2020). CL-37 is shown here to correlate with the Late Holocene caldera-forming eruption of Opala (OP), Kamchatka (Andrews et al., 2018; Braitseva et al., 1995, 1997; Kyle et al., 2011; Melekestsev et al., 1992; Plunkett et al., 2015). CL-37 is the first ultra-distal correlation of glass from this eruption outside of Kamchatka.

Here we report an updated modelled eruption age for OP of 1395–1305 cal yr BP (Fig. S4). This was produced using the Tau_Boundary function in OxCal v4.4 with IntCal20 following the methodology of Davies et al. (2016) with $^{14}C$ ages reported in Braitseva et al. (1995) (Table S5). This is in good agreement with previous published ages for the eruption but is younger than the radiometric age-model estimate for this depth by ∼ 1470–1950 years (Table S6).

### 3.2 Multimodal/mixed glass populations

Glass shards from six of the remaining analysed shard peaks have mixed or multimodal geochemical data, and two have scattered results with no discernible trend. It should be noted here that there are many recorded examples of heterogenous melts with bimodal geochemical trends from Alaska volcanoes (e.g. Aniakchak CFE II, Novarupta–Katmai 1912; see Table S2). However, none of the multi-model samples reported here are interpreted in this way as the different populations do not follow any geochemical trends that would be expected if they were from the same eruption. Instead, they form distinct geochemical populations that more likely represent multiple eruptions from different sources.

Higher levels of background shards are present from 35 cm to the surface, and the geochemical "noise" is also particularly evident in the youngest samples, with all peaks analysed in the past millennium showing either multimodal (> five glass geochemical populations) or scattered data. Detailed geochemical biplots for multimodal sample populations, including those with only a few shards (e.g. CL-0, CL-2, CL-31, CL-61), are shown in Fig. S5. Glass shards from these samples display a mix of morphologies (including platy, cuspate, vesicular and microlitic), which are all commonly seen in tephra in this area. Their grain sizes do not show any differentiation between types (as also seen for the unimodal samples discussed above); these data cannot therefore be used to identify any differences between subpopulations of these samples.

CL-61 is the only analysed mixed sample that predates the past millennium, located between the Ruppert (CL-74, 2800–2130 cal yr BP) and WRAn (CL-48, 1689–1560 cal yr BP) tephras. It has a final age–depth model estimated age of 2450–1700 cal yr BP ($2\sigma$; Table S7). It contains a few shards that are similar to the rhyodacite from Aniakchak volcano and also an Augustine tephra (Fortin et al., 2019; Waitt and Begét, 2009), but while these volcanoes have known activity at this time (e.g. Bacon et al., 2014; Waitt and Begét, 2009), there are not enough analyses available for a confident correlation.

Of the six mixed samples, only two – CL-4 (180–60 cal yr BP, $2\sigma$, Table S7) and CL-7 (625–75 cal yr BP, $2\sigma$, Table S7) – have populations that can be identified as dominant from the analyses presented here. Rhyodacitic and

dacitic glass shards from these samples overlap geochemically with reference data for Aniakchak (Davies et al., 2016) and are interpreted as strong evidence of eruptive activity at Aniakchak, given both the number of shards and the proportion of analyses that they represent. CL-7 also has six points that are geochemically similar to the Early Holocene eruption KO (∼ 8410–8455 cal yr BP; Braitseva et al., 1997) from Kamchatka, but this does not correlate to any known eruptions from Kamchatka in the timeframe of this deposit. While these are the three most coherent geochemical populations observed in these mixed samples, they are not deemed useful here for chronostratigraphic applications (discussed further in the "Multimodal samples and historical activity" section).

An alternative approach for considering these mixed data is to parse by geochemical trend that can be broadly related to a source rather than to any individual eruption. Given the high levels of background shards it is possible that the chosen shard concentration peaks do not relate directly to primary tephra fall. This is particularly likely where multiple eruptive events are closely spaced in time and therefore overlap within the temporal resolution of 1 cm of sediment accumulation. As each sample might contain shards from multiple eruptions these data can be seen as recording eruptive activity in a broader period, instead of discrete eruptions or accurately dated events.

Using this source-based classification, it is possible to identify eight geochemical groups, illustrated in Fig. 4, for the four mixed samples from the past ∼ 1000 years, CL-31 and CL-61. Five of these eight geochemical groups correlate with reference glass data for volcanic sources in Alaska (Aniakchak, Mt Churchill, Redoubt Volcano, Augustine Volcano, Mt Katmai). These volcanoes all have known eruptions or suspected eruptive activity during this time period (e.g. Cameron et al., 2020).

## 4 Bayesian age modelling

Step one of our chronometer comparison (see Sect. 2.3) considered where the individual ages fit their expected stratigraphic order. Steen (2016) noted that two $^{14}$C ages from the full core sequence (5.5–7.5 cm and 245–248 cm) were anomalously old compared to their surrounding ages and these were therefore excluded from further consideration. While the $^{210}$Pb ages are not discussed here in detail (given their limited applicability to the Late Holocene record), they overlap with the youngest $^{14}$C age (2.6–4.5 cm). They therefore help constrain the broad age range (295–60 cal yr BP) of this sample that sits on a plateau in the radiocarbon calibration curve.

For step two of our comparison, an overlay of the individually modelled chronometers shows that there are substantial offsets between three of the five $^{14}$C ages from this portion of the core and the four available cryptotephra-correlated ages (Fig. 5). We place a high level of confidence in these tephra-correlated ages as the four identified tephra are well characterised, widely identified in other depositional records (both intra- and extra-regionally) and in a logical stratigraphic context in relation to one another. The radiometric model also had very low agreement (Amodel = 10.3; individual age AI values range from 19.7–78.8), indicating a likely issue within the dataset. Hence, two further $^{14}$C ages (30.5–32.5 cm, 85.75–87.75 cm) are also identified as anomalously old and removed here as outliers. Given the trend in the correlated tephra age model, the lower 138–140 cm $^{14}$C age may also be slightly old (unless, for example, there is an unexpected change in sedimentation rates in this part of the core). However, as there are no tephra-correlated ages within 30 cm of this $^{14}$C sample, this could not be confirmed at this stage.

For step three of the comparison, a P_Sequence model was produced (OxCal v4.4., Bronk Ramsey 2009a) that incorporates the remaining data. As Steen (2016) demonstrated better agreement between their chronometers below 2 m depth, $^{14}$C ages for the rest of the sequence (down to 3.51 m; Table 1, Fig. 2a) are also included here. The data initially included in the model were six $^{210}$Pb ages, four tephra-correlated ages and seven $^{14}$C ages. For this step, both OxCal's agreement indices and a general Student's $t$ test were used to statistically identify outliers. The initial combined P_Sequence model had good model agreement (Amodel = 81.5) and no further $^{14}$C dates were identified as outliers by Student's $t$ test. The two oldest $^{14}$C dates (303–304 cm, 348.5–351 cm) have posterior values that are slightly over the set threshold (9 and 6 respectively compared to the prior of 5) but are not excluded here.

A final model for CASC-4A/2D is shown in Fig. 6. Below the top 4 cm, six ages (four correlated tephra, two $^{14}$C) are used to date down to 1.4 m (∼ 6 ka), providing a robust age model for this portion of the lake sediments. Four $^{14}$C ages are used for 1.4–3.51 m (∼ 9 ka, 6–15 ka) of the sequence, and as there are no independent tephra data for this section, these data are reported as provisional. Additional data – especially from independent chronometers – would increase confidence in the lower half of this model.

## 5 Discussion

The data reported here have implications for cryptotephra records in northwestern North America and for Arctic sedimentary sequences and age models through the successful application of multi-chronometer Bayesian age modelling.

### 5.1 Cryptotephra in Arctic Alaska

This study demonstrates that identifiable concentrations of volcanic glass reach the north flank of the Brooks Range and can be used as chronostratigraphic tools where clear evidence of primary tephra fall is preserved (see Sect. 5.2. for a discussion of this caveat). In particular, this is the first report of ultra-distal glass from the Late Holocene eruption of Opala,

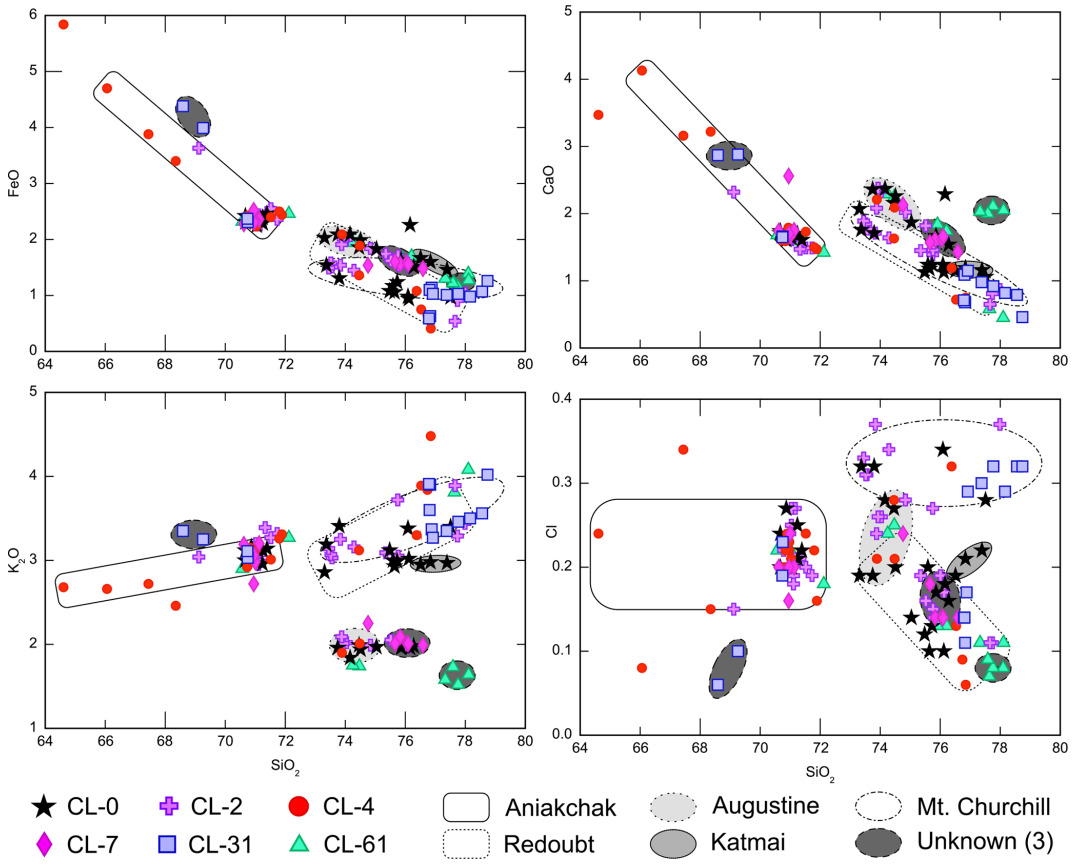


**Figure 4.** Geochemical biplots showing mixed-glass samples from Cascade Lake. Bounding shapes represent simplified geochemical fields for potential source volcanoes (to aid visualisation). For the full glass geochemical-data ranges associated with these volcanic sources see Bolton et al. (2020), Davies et al. (2016), Fortin et al. (2019) and Zander et al. (2018). Three populations with unknown sources are also shown using the same bounding line and fill. All single-point analysis data are listed in Table S2.

Kamchatka (> 3000 km from Cascade Lake), as well as an unknown tephra, CL-96, likely from a source in the Alaska Peninsula–Aleutian Arc. Ruppert tephra and Aniakchak CFE II are both documented on the southern slope of the Brooks Range (Monteath et al., 2017), and their distributions are expanded here across this large topographic barrier. This is also the first distal identification of WRAn this far to the northwest of Mt Churchill.

Glass shard morphologies and preliminary grain size measurement data are reported for the unimodal tephra populations at Cascade Lake. However, these data are not used here to differentiate between samples or subpopulations – for example, the five tephra with distinct geochemical populations all have similar maximum axis length and sphericity values. This is not surprising for maximum axis length, as previous studies have shown that the grain sizes reported here (20–40 µm) are commonly found in deposits located 500–3000 km from their source (Stevenson et al., 2015). Quantitative grain size measurements provide valuable information for a range of research questions but are not commonly reported for cryptotephra (Saxby et al., 2020). Hence, these data are provided here as preliminary values for distal deposits of these correlated tephra.

While the cryptotephra profile here only covers the Late Holocene, it highlights eruptive events that are both locally important and widespread and provides possibilities for correlating proxy data within North America and across the Pacific in Kamchatka. Our focus was specifically on the past ∼ 4 kyr as there are several widespread, well-dated and geochemically characterised tephra within Alaska during this time period. From 12–4 ka, there is a paucity of well-dated regional tephra that is documented and fully characterised, but it is possible that new tephra from other regions may be identified as more tephra studies are published, as seen here with OP.

Compared to the cryptotephra stratigraphies published in Monteath et al. (2017) from Ruppert Lake and Woody Bog Pond, located ∼ 150 km south of Cascade Lake on the southern slope of the Brooks Range, large differences can be seen in both the amount of primary tephra preserved and the overall shard presence and concentrations. Reported glass abundances at the southern sites are at least an order of magnitude

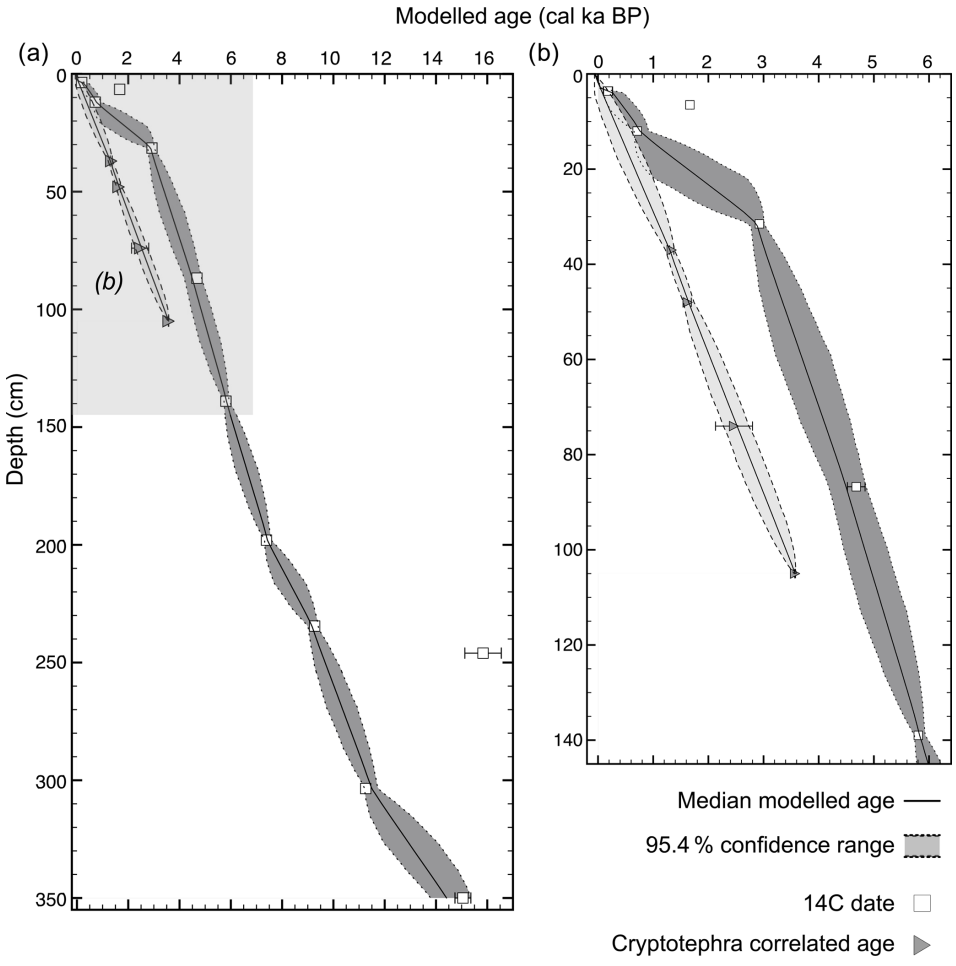


**Figure 5.** Cascade Lake core CASC-4A/2D multi-method chronometer comparison of downcore age models based on radiocarbon ages (dark grey shading) and correlated tephra ages (data are reported in Table S6). Two sigma uncertainties are plotted for all samples; where bars are not visible, the uncertainty is smaller than the symbol. **(a)** All $^{14}$C dates produced by Steen (2016) from CASC-4A/2D; **(b)** the focused upper section with new cryptotephra analyses from this study.

higher than those from Cascade Lake (hundreds to thousands vs. tens of shards $g^{-1}$ or less). This likely relates in part to the topographic barrier presented by the Brooks Range, causing increased rain-out of shards being transported from the south (e.g. in north-trending plumes from Aniakchak CFE II) and deposition of shards before they reach the northern slope (e.g. Watt et al., 2015). Other factors may include lake size and bathymetry, catchment size, local topography and hydrology (e.g. Pyne-O'Donnell, 2010). Cascade Lake is an order of magnitude larger and deeper than the southern sites and hence has a larger surface area ($\sim 1$ vs. 0.04 and 0.01 $km^2$), but its catchment area is not proportionally larger ($\sim 10$ vs. $< 4\,km^2$) and it has no current inflow. Hence, it is suggested here that topography is a primary influence on Cascade Lake shard concentrations (compared to other sites further south) and not lake characteristics.

There are common issues affecting cryptotephra research in Alaska that still apply at this distal, Arctic site. Cascade Lake is downwind of multiple active volcanic sources where records show that multiple closely spaced eruptions have occurred. This, combined with relatively low sediment accumulation rates, is likely to cause geochemical variability within individual samples where 1 cm of sediment represents decades of accumulation (25–67 $yr\,cm^{-1}$ calculated for Cascade Lake's 15 ka age–depth model). The presence of glass in $\sim 75$ % of the samples analysed here shows a level of background deposition that must be considered when interpreting data from identified shard concentration peaks. This is particularly important here as (a) the peak concentrations are relatively low compared to other cryptotephra records in the region (e.g. Davies, 2018; Monteath et al., 2017; Payne and Blackford, 2004) and (b) the signal-to-noise ratio between peaks that have been correlated with known eruptions and the (fairly consistent) background shard concentration is relatively high. Reworking and secondary deposition of tephra in the landscape can also be a substantial issue for records

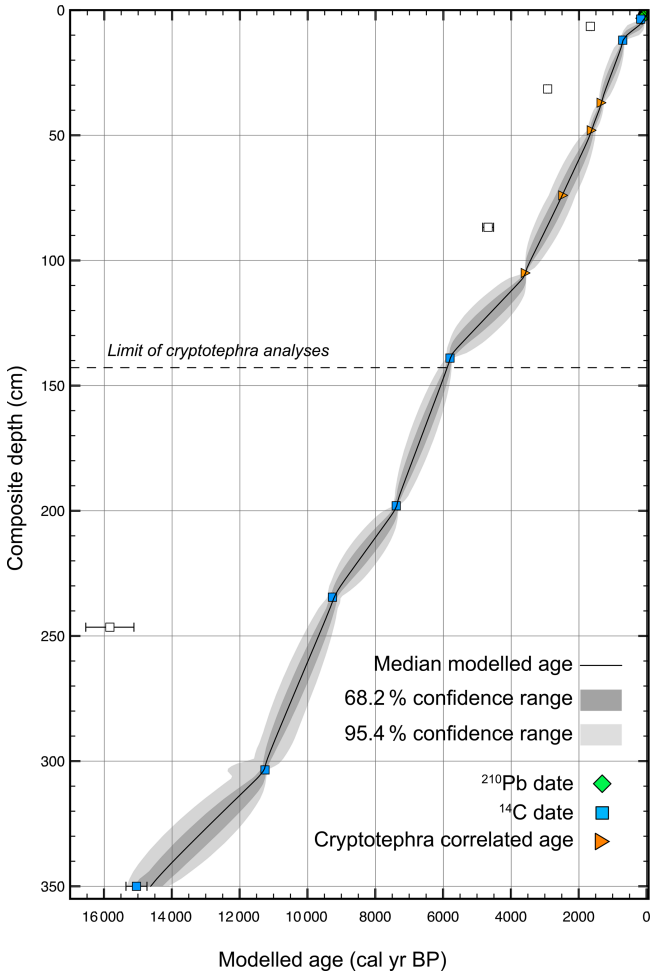


**Figure 6.** Age–depth plot showing the final Bayesian age model for Cascade Lake composite core CASC-4A/2D. Shaded areas show the $1\sigma$ (68.2 %) and $2\sigma$ (95.4 %) confidence ranges. Filled symbols are included in the model and white symbols are identified as outliers. Two sigma errors are included for all ages; where they are not visible the error is smaller than the symbol used. Full details and values can be found in Table S7.

from this region, but this is not a likely problem at Cascade Lake as there is so little tephra present in the area (i.e. there is no clear source for tephra to be reworked from).

Furthermore, a broader issue that affects how much confidence can be attributed to a geochemical correlation is the available glass data for reference material from given eruptions or volcanoes. Here, this is relatively limited in scope compared to the number of Late Holocene eruptions reported in Alaska. Comparisons are often made with tephra data that relate to a small number of eruptions (or possibly only one) from a subset of the volcanoes with known activity. A degree of uncertainty will therefore affect correlations with given eruptions or sources until more characterisations are published from both proximal and distal tephra deposits.

### 5.2 Multimodal samples and historical activity

The issue of clear evidence of primary tephra fall being preserved is one that affects all cryptotephra records. Low numbers of shard analyses cannot be interpreted as conclusive evidence of an eruption, especially if multiple geochemical populations or trends are observed. This appears to only be a problem for certain parts of the Cascade Lake tephrostratigraphic record; there are discernible changes in shard concentrations and sample compositions from the younger portion of the core. For example, samples analysed from 0–30 cm have multiple geochemical populations, which are not frequently seen below this. This is likely related to an overall increase in the shard concentrations and peak density that is particularly notable for the top 15 cm of the core. These differences could be the result of a myriad of regional (e.g. weather patterns) and local (e.g. reworking) factors that affect the distribution and preservation of shards (e.g. Watson et al., 2015), but at Cascade Lake we hypothesise this may largely be the result of changing sedimentation rates.

Overall, it is possible that the background shards evident in the full Cascade Lake shard concentration profile (Fig. 2b) could be the result of taphonomic problems such as reworking, bioturbation or secondary in-wash. However, this is not likely a substantial problem for the record presented here. The lake sediments are laminated and do not show signs of deformation (from either in situ processes or the core extraction). These shards are also unlikely to represent significant reworking from the surrounding landscape, or within the lake sediment itself, as there is little ash in the area and therefore no obvious source for redeposition. Furthermore, the tails and multiple peaks do not show repetition of a common geochemical signal, which would be expected if the shards were reworked or secondary in-wash (e.g. as seen with Askja 1875 in the Swedish lakes Spåime and Getvaltjärnen, reported by Davies et al., 2007, or with the eastern lobe of the White River Ash at Sydney Bog in Jensen et al., 2021).

Geochemical data from the top 30 cm do show some repetition between samples, so it is not possible to rule out reworking for this portion of the core, but this may also be the result of multiple eruptions from single sources in this $\sim$ 1000-year time period. Sedimentation rates are relatively low at this site, particularly for this interval at 30–67 yr cm$^{-1}$ (Table S7), which would cause increased overlap for closely spaced events. Hence, the glass shard data from the last $\sim$ 1000 years are interpreted as evidence for trace amounts of tephra reaching the north flank of the Brooks Range. Beyond the five clearly defined cryptotephra samples described above, we present evidence of volcanic activity from Augustine, Redoubt, Aniakchak, Mt Churchill, Mt Katmai (e.g. Bolton et al., 2020) and further possible sources in Kamchatka and Alaska based on geochemical similarities to available reference data for characterised eruptions (Fig. 4). This supposition is supported by records of eruptions from the past millennium (e.g. Cameron et al., 2020), which include

Novarupta–Katmai 1912, six eruptions from Redoubt and 14 from Augustine. A higher sampling resolution for this period may help distinguish individual eruptive events and resolve this question, but with such low sedimentation rates it may instead highlight the limit of this record's preservation potential.

Eruptions in the past millennium from both Mt Churchill and Aniakchak have been identified distally elsewhere in Alaska. For Mt Churchill there is published evidence for an eruption in the last 500 years: the Lena tephra is dated to 310–285 cal yr BP (Payne et al., 2008). It is possible that shards from CL-0 and CL-2 relate to this tephra, but their modelled age is too young to support a correlation (1930–2010 CE). Proximal records at Aniakchak indicate multiple eruptions have occurred between 560 to 70 BP (Bacon et al., 2014; Neal et al., 2001), and a distal tephra in the Akhlun Mountains, southwest Alaska is dated at around 400 BP (Kaufman et al., 2012). The large number of analyses that geochemically correlate with Aniakchak (47, including 4 dacitic points) over four samples from Cascade Lake (CL-0, CL-2, CL-4 and CL-7) are interpreted here as representing at least one eruptive event in the last $\sim$ 400 years. However, any correlations here are limited by both the lack of glass geochemical data on proximal tephra and the high uncertainty in modelled ages for these samples at Cascade Lake. Our age model places these samples between 630 and 10 cal yr BP ($2\sigma$) due to decreased sedimentation rates at this time, so additional correlation(s) with other younger eruption(s) from Aniakchak also cannot be ruled out.

### 5.3 Cascade Lake age models

It is not uncommon for ages produced by multiple chronometers to diverge over part or all of a sediment sequence. Individual chronometers have their own inherent strengths and weaknesses, and their different physical properties can be affected by a number of different processes, which in turn affect the preserved and eventually measured signal (e.g. Davies et al., 2018). This is somewhat disheartening as using multiple techniques should provide a check for bias and inaccurate data, but additional independent data can be used to identify and reconcile observed offsets, as shown here.

Once any obvious outliers have been addressed (i.e. step one from Sect. 2.3), it is not always easy to resolve any remaining disagreements between chronometers. Here, the importance of independent chronological validation from marker horizons (Late Holocene cryptotephra, which provide additional data in a key period) and the power of Bayesian statistical approaches for age modelling are demonstrated. The identification of periods of offset and anomalous or biased ages can allow further investigation of the potential causes, such as mechanical (e.g. mobilisation or redeposition) or chemical (e.g. alteration or degradation) processes affecting the analysed sample material. In this case, however, the resulting age–depth model for the whole core can still be strengthened by the addition of further independent chronological data, especially for the lower section (1.42–3.51 m).

The commonly applied method of $^{14}$C dating can have low reported uncertainties but is restricted at some Arctic sites by a lack of suitable material. Where macrofossils are available, they may be affected by old carbon contamination or the redeposition of older material. Cascade Lake's location in limestone terrain likely resulted in a hard-water effect, which could explain the anomalously old $^{14}$C ages identified here: four of the Holocene $^{14}$C ages are variably 500–5000 years too old compared to median modelled ages for their given depths. As mentioned in other studies the use of either terrestrial material or the humic fraction of sediment is recommended, especially when in limestone terrane (Lowe and Walker, 2000). Nonetheless, this study adds to a growing body of literature that demonstrates that using multiple independent chronometers with Bayesian age-modelling techniques can produce accurate and reliable age–depth models for Arctic lake sediments.

## 6 Conclusions

This research demonstrates the potential for dating Arctic lake sediments in Alaska using cryptotephra correlations. The advantages of tephrochronology include the relatively long period of time over which it can be applied (compared to $^{210}$Pb and $^{14}$C), the level of precision associated with known tephra ages (especially those from documented historical events), and the potential for independently testing and validating other chronometers with tephra-correlated ages. We suggest here that the most robust age models can be produced by using a combination of chronostratigraphic techniques in a Bayesian statistical model. While cryptotephra are best defined regionally for the Late Holocene, it is possible that other well-dated cryptotephra from Alaska (e.g. the Early Holocene caldera-forming eruptions from Fisher, Stelling et al., 2005; the Late Pleistocene Tephra D, Davies et al., 2016) and ultra-distal sources (e.g. Kamchatka, Japan) could be identified in northern regions.

**Data availability.** The major-element glass geochemistry data and associated metadata for individual tephra grains will be made available publicly though the Alaska Volcano Observatory Geochemical Database at https://www.avo.alaska.edu/geochem/ (last access: 23 February 2022; Cameron et al., 2019; https://doi.org/10.14509/30058), part of the larger Geologic Database of Information on Volcanoes in Alaska (GeoDIVA). The Bayesian age–depth models generated in this study, including the underlying radiometric ages are available as the Supplement.

**Supplement.** The supplement related to this article is available online at: https://doi.org/10.5194/gchron-4-121-2022-supplement.

**Author contributions.** LJD carried out the research, helped conceptualise the study and wrote the paper. DSK and BJLJ helped conceptualise and fund the study and revised the paper. DSK provided the samples. BJLJ carried out some of the analyses.

**Competing interests.** At least one of the (co-)authors is a member of the editorial board of *Geochronology*. The peer-review process was guided by an independent editor, and the authors also have no other competing interests to declare.

**Disclaimer.** Publisher's note: Copernicus Publications remains neutral with regard to jurisdictional claims in published maps and institutional affiliations.

**Acknowledgements.** Many thanks to everyone who has been involved in producing the data discussed within this paper. Jason Briner, David Fortin and Liz Ceperley helped core Cascade Lake; LacCore staff assisted with the initial core analysis and curation. Flett Research, Ltd. provided the $^{210}$Pb measurements and the W. M. Keck Carbon Cycle Accelerator Mass Spectrometry Laboratory at UC-Irvine provided the $^{14}$C measurements. Vera Ponomareva discussed and plotted reference data for an initial comparison with Kamchatkan tephra data. Ben Andrews supplied reference material from Opala tephra that was analysed at the University of Alberta. Josephine Bailey assisted with image analysis methodologies and grain size calculations.

**Financial support.** This research has been supported by the National Science Foundation (grant no. 1107662) and the Natural Sciences and Engineering Research Council of Canada (Discovery grant no. RGPIN-2018-04926 and Accelerator grant no. RGPAS-2018-52250), and Lauren J. Davies has been supported by the Leverhulme Trust through an Early Career Fellowship since October 2020.

**Review statement.** This paper was edited by Richard Staff and reviewed by Kristi Wallace and two anonymous referees.

## References

Abbott, P., Bonnadonna, C., Bursik, M., Cashman, K., Davies, S., Jensen, B., Kuehn, S., Kurbatov, A., Lane, C., Plunkett, G., Smith, V., Thomlinson, E., Thordarsson, T., Walker, J. D., and Wallace, K.: Community Established Best Practice Recommendations for Tephra Studies-from Collection through Analysis (3.0.0), Zenodo [data set], https://doi.org/10.5281/zenodo.5047775, 2021.

Adolphi, F. and Muscheler, R.: Synchronizing the Greenland ice core and radiocarbon timescales over the Holocene – Bayesian wiggle-matching of cosmogenic radionuclide records, Clim. Past, 12, 15–30, https://doi.org/10.5194/cp-12-15-2016, 2016.

Ager, T. A.: Late Quaternary vegetation and climate history of the central Bering land bridge from St. Michael Island, western Alaska, Quaternary Res., 60, 19–32, https://doi.org/10.1016/S0033-5894(03)00068-1, 2003.

Alaska Volcano Observatory: Alaska Volcano Observatory Online Library, https://avo.alaska.edu/volcanoes/index.php (last access: 23 February 2022), 2016.

Andrews, B. J., Dufek, J., and Ponomareva, V.: Eruption dynamics and explosive-effusive transitions during the 1400 cal BP eruption of Opala volcano, Kamchatka, Russia, J. Volcanol. Geoth. Res., 356, 316–330, https://doi.org/10.1016/j.jvolgeores.2018.02.019, 2018.

Appleby, P. G. and Oldfield, F.: The calculation of lead-210 dates assuming a constant rate of supply of unsupported $^{210}$Pb to the sediment, Catena, 5, 1–8, https://doi.org/10.1016/S0341-8162(78)80002-2, 1978.

Bacon, C. R., Neal, C. A., Miller, T. P., McGimsey, R. G., and Nye, C. J.: Postglacial eruptive history, geochemistry, and recent seismicity of Aniakchak volcano, Alaska Peninsula, U.S. Geological Survey, Professional Paper 1810, 74 pp., https://doi.org/10.3133/pp1810, 2014.

Baillie, M. G. L. and McAneney, J.: Tree ring effects and ice core acidities clarify the volcanic record of the first millennium, Clim. Past, 11, 105–114, https://doi.org/10.5194/cp-11-105-2015, 2015.

Barletta, F., St-Onge, G., Channell, J. E. T., Rochon, A., Polyak, L., and Darby, D.: High-resolution paleomagnetic secular variation and relative paleointensity records from the western Canadian Arctic: implication for Holocene stratigraphy and geomagnetic field behaviour, Can. J. Earth Sci., 45, 1265–1281, https://doi.org/10.1139/E08-039, 2008.

Blaauw, M. and Christen, J. A.: Radiocarbon peat chronologies and environmental change, J. R. Stat. Soc. C-Appl., 54, 805–816, https://doi.org/10.1111/j.1467-9876.2005.00516.x, 2005.

Blackford, J. J., Payne, R. J., Heggen, M. P., de la Riva Caballero, A., and van der Plicht, J.: Age and impacts of the caldera-forming Aniakchak II eruption in western Alaska, Quaternary Res., 82, 85–95, https://doi.org/10.1016/j.yqres.2014.04.013, 2014.

Blockley, S. P. E., Pyne-O'Donnell, S. D. F., Lowe, J. J., Matthews, I. P., Stone, A., Pollard, A. M., Turney, C. S. M., and Molyneux, E. G.: A new and less destructive laboratory procedure for the physical separation of distal glass tephra shards from sediments, Quaternary Sci. Rev., 24, 1952–1960, https://doi.org/10.1016/j.quascirev.2004.12.008, 2005.

Blockley, S. P. E., Bronk Ramsey, C., and Pyle, D. M.: Improved age modelling and high-precision age estimates of late Quaternary tephras, for accurate palaeoclimate reconstruction, J. Volcanol. Geoth. Res., 177, 251–262, https://doi.org/10.1016/j.jvolgeores.2007.10.015, 2007.

Blockley, S. P. E., Edwards, K. J., Schofield, J. E., Pyne-O'Donnell, S. D. F., Jensen, B. J. L., Matthews, I. P., Cook, G. T., Wallace, K. L., and Froese, D.: First evidence of cryptotephra in palaeoenvironmental records associated with Norse occupation sites in Greenland, Quat. Geochronol., 27, 145–157, https://doi.org/10.1016/j.quageo.2015.02.023, 2015.

Bolton, M., Jensen, B. J. L., Wallace, K. L., Praet, N., Fortin, D., Kaufman, D. S., and De Batist, M.: Machine learning classifiers for attributing tephra to source volcanoes: An evaluation of methods for Alaska tephras, J. Quaternary Sci., In-revisio, 35, 81–92, https://doi.org/10.1002/jqs.3170, 2020.

Braitseva, O. A., Melekestsev, I. V., Ponomareva, V. V., and Sulerzhitsky, L. D.: Ages of calderas, large explosive craters and active volcanoes in the Kuril-Kamchatka region, Russia, B. Volcanol., 57, 383–402, https://doi.org/10.1007/BF00300984, 1995.

Braitseva, O. A., Ponomareva, V. V., Sulerzhitsky, L. D., Melekestsev, I. V., and Bailey, J.: Holocene Key-Marker Tephra Layers in Kamchatka, Russia, Quaternary Res., 47, 125–139, https://doi.org/10.1006/qres.1996.1876, 1997.

Brock, F., Lee, S., Housley, R. A., and Bronk Ramsey, C.: Variation in the radiocarbon age of different fractions of peat: A case study from Ahrenshöft, northern Germany, Quat. Geochronol., 6, 550–555, https://doi.org/10.1016/j.quageo.2011.08.003, 2011.

Bronk Ramsey, C.: Deposition models for chronological records, Quaternary Sci. Rev., 27, 42–60, https://doi.org/10.1016/j.quascirev.2007.01.019, 2008.

Bronk Ramsey, C.: Bayesian Analysis of Radiocarbon Dates, Radiocarbon, 51, 337–360, https://doi.org/10.1017/S0033822200033865, 2009a.

Bronk Ramsey, C.: Dealing with Outliers and Offsets in Radiocarbon Dating, Radiocarbon, 51, 1023–1045, https://doi.org/10.1017/S0033822200034093, 2009b.

Bronk Ramsey, C. and Lee, S.: Recent and Planned Developments of the Program OxCal, Radiocarbon, 55, 720–730, https://doi.org/10.1017/S0033822200057878, 2013.

Cameron, C. E., Mulliken, K. M., Crass, S. W., Schaefer, J. R., and Wallace, K. L.: Alaska Volcano Observatory geochemical database, version 2, Alaska Division of Geological & Geophysical Surveys [data set], Digital Data Series 8 v. 2, 22 pp., https://doi.org/10.14509/30058, 2019 (data available at: https://www.avo.alaska.edu/geochem/, last access: 23 February 2022).

Cameron, C. E., Schaefer, J. R., and Ekberg, P. G.: Historically active volcanoes of Alaska, Alaska Division of Geological & Geophysical Surveys [data set], Miscellaneous Publication 133 v. 4, 2 sheets, https://doi.org/10.14509/30426, 2020.

Christen, J. A., Clymo, R. S., and Litton, C. D.: A Bayesian Approach to the Use of $^{14}$C Dates in the Estimation of the Age of Peat, Radiocarbon, 37, 431–441, https://doi.org/10.1017/S0033822200030915, 1995.

Cook, E., Portnyagin, M., Ponomareva, V., Bazanova, L., Svensson, A., and Garbe-Schönberg, D.: First identification of cryptotephra from the Kamchatka Peninsula in a Greenland ice core: Implications of a widespread marker deposit that links Greenland to the Pacific northwest, Quaternary Sci. Rev., 181, 200–206, https://doi.org/10.1016/j.quascirev.2017.11.036, 2018.

Coulter, S. E., Pilcher, J. R., Plunkett, G., Baillie, M., Hall, V. A., Steffensen, J. P., Vinther, B. M., Clausen, H. B., and Johnsen, S. J.: Holocene tephras highlight complexity of volcanic signals in Greenland ice cores, J. Geophys. Res.-Atmos., 117, 1–11, https://doi.org/10.1029/2012JD017698, 2012.

Cox, A.: Latitude Dependence of the Angular Dispersion of the Geomagnetic Field, Geophys. J. Roy. Astr. S., 20, 253–269, https://doi.org/10.1111/j.1365-246X.1970.tb06069.x, 1970.

Davies, L. J.: The development of a Holocene cryptotephra framework in northwestern North America, University of Alberta, https://doi.org/10.7939/R3HX1660C, 2018.

Davies, L. J., Jensen, B. J. L., Froese, D. G., and Wallace, K. L.: Late Pleistocene and Holocene tephrostratigraphy of interior Alaska and Yukon: Key beds and chronologies over the past 30,000 years, Quaternary Sci. Rev., 146, 28–53, https://doi.org/10.1016/j.quascirev.2016.05.026, 2016.

Davies, L. J., Appleby, P., Jensen, B. J. L., Magnan, G., Mullan-Boudreau, G., Noernberg, T., Shannon, B., Shotyk, W., van Bellen, S., Zaccone, C., and Froese, D. G.: High-resolution age modelling of peat bogs from northern Alberta, Canada, using pre- and post-bomb $^{14}$C, $^{210}$Pb and historical cryptotephra, Quat. Geochronol., 47, 138–162, https://doi.org/10.1016/j.quageo.2018.04.008, 2018.

Davies, L. J., Jensen, B. J. L., and Locock, A. J.: Do visible Holocene tephra from Mt. Churchill, Alaska, display varying geochemistry across their distributions?, in: INQUA XX Congress, Dublin, Ireland, 25–31 July 2019, P-1609, https://doi.org/10.13140/RG.2.2.25337.13921, 2019.

Davies, S. M.: Cryptotephras: The revolution in correlation and precision dating, J. Quaternary Sci., 30, 114–130, https://doi.org/10.1002/jqs.2766, 2015.

Davies, S. M., Elmquist, M., Bergman, J., Wohlfarth, B., and Hammarlund, D.: Cryptotephra sedimentation processes within two lacustrine sequences from west central Sweden, Holocene, 17, 319–330, https://doi.org/10.1177/0959683607076443, 2007.

de Fontaine, C. S., Kaufman, D. S., Scott Anderson, R., Werner, A., Waythomas, C. F., and Brown, T. A.: Late Quaternary distal tephra-fall deposits in lacustrine sediments, Kenai Peninsula, Alaska, Quaternary Res., 68, 64–78, https://doi.org/10.1016/j.yqres.2007.03.006, 2007.

Denton, J. S. and Pearce, N. J. G.: Comment on "A synchronized dating of three Greenland ice cores throughout the Holocene" by B. M. Vinther et al.: No Minoan tephra in the 1642 B. C. layer of the GRIP ice core, J. Geophys. Res.-Atmos., 113, 1–7, https://doi.org/10.1029/2007JD008970, 2008.

Deschamps, C. E., St-Onge, G., Montero-Serrano, J. C., and Polyak, L.: Chronostratigraphy and spatial distribution of magnetic sediments in the Chukchi and Beaufort seas since the last deglaciation, Boreas, 47, 544–564, https://doi.org/10.1111/bor.12296, 2018.

Donovan, J., Kremser, D., Fournelle, J. H., and Goemann, K.: Probe for EPMA: Acquisition, automation and analysis, https://www.probesoftware.com (last access: 23 February 2022), 2015.

Fierstein, J.: Explosive eruptive record in the Katmai region, Alaska Peninsula: An overview, B. Volcanol., 69, 469–509, https://doi.org/10.1007/s00445-006-0097-y, 2007.

Foo, Z. H., Jensen, B. J. L., and Bolton, M. S. M.: Glass geochemical compositions from widespread tephras erupted over the last 200 years from Mount St. Helens, J. Quaternary Sci., 35, 102–113, https://doi.org/10.1002/jqs.3166, 2020.

Fortin, D., Praet, N., McKay, N. P., Kaufman, D. S., Jensen, B. J. L., Haeussler, P. J., Buchanan, C., and De Batist, M.: New approach to assessing age uncertainties – The 2300 year varve chronology from Eklutna Lake, Alaska (USA), Quaternary Sci. Rev., 203, 90–101, https://doi.org/10.1016/j.quascirev.2018.10.018, 2019.

Gaglioti, B. V., Mann, D. H., Jones, B. M., Pohlman, J. W., Kunz, M. L., and Wooller, M. J.: Radiocarbon age-offsets in an arctic lake reveal the long-term response of permafrost carbon to climate change, J. Geophys. Res.-Biogeo., 119, 1630–1651, https://doi.org/10.1002/2014JG002688, 2014.

Global Volcanism Program: Volcanoes of the World, v. 4.8.0., https://doi.org/10.5479/si.GVP.VOTW4-2013, 2013.

Harvey, J. R.: Cryptotephra deposition and preservation in four sub-Arctic lakes in Yukon, Canada, University of Alberta, https://doi.org/10.7939/r3-80dy-ww06, 2021.

Hua, Q., Turnbull, J. C., Santos, G. M., Rakowski, A. Z., Ancapichún, S., De Pol-Holz, R., Hammer, S., Lehman, S. J., Levin, I., Miller, J. B., Palmer, J. G., and Turney, C. S. M.: Atmospheric Radiocarbon for the Period 1950–2019, Radiocarbon, 1–23, https://doi.org/10.1017/RDC.2021.95, 2021.

Jensen, B. J. L.: Tephrochronology of middle to late Pleistocene loess in east-central Alaska, MSc thesis, University of Alberta, Edmonton, Alberta, Canada, https://doi.org/10.7939/r3-tqyv-zf79, 2007.

Jensen, B. J. L., Froese, D. G., Preece, S. J., Westgate, J. A., and Stachel, T.: An extensive middle to late Pleistocene tephrochronologic record from east-central Alaska, Quaternary Sci. Rev., 27, 411–427, https://doi.org/10.1016/j.quascirev.2007.10.010, 2008.

Jensen, B. J. L., Pyne-O'Donnell, S., Plunkett, G., Froese, D. G., Hughes, P. D. M., Sigl, M., McConnell, J. R., Amesbury, M. J., Blackwell, P. G., van den Bogaard, C., Buck, C. E., Charman, D. J., Clague, J. J., Hall, V. A., Koch, J., Mackay, H., Mallon, G., McColl, L., and Pilcher, J. R.: Transatlantic distribution of the Alaskan White River Ash, Geology, 42, 875–878, https://doi.org/10.1130/G35945.1, 2014.

Jensen, B. J. L., Beaudoin, A. B., Clynne, M. A., Harvey, J., and Vallance, J. W.: A re-examination of the three most prominent Holocene tephra deposits in western Canada: Bridge River, Mount St. Helens Yn and Mazama, Quatern. Int., 500, 83–95, https://doi.org/10.1016/j.quaint.2019.03.017, 2019.

Jensen, B. J. L., Davies, L. J., Nolan, C., Pyne-O'Donnell, S., Monteath, A. J., Ponomareva, V., Portnyagin, M., Booth, R., Bursik, M., Cook, E., Plunkett, G., Vallance, J. W., Luo, Y., Cwynar, L. C., Hughes, P., and Pearson, D. G.: A latest Pleistocene and Holocene composite tephrostratigraphic framework for northeastern North America, Quaternary Sci. Rev., 272, 107242, https://doi.org/10.1016/j.quascirev.2021.107242, 2021.

Karrow, P. F. and Anderson, T. W.: Palynological Study of Lake Sediment Profiles from Southwestern New Brunswick: Discussion, Can. J. Earth Sci., 12, 1808–1812, https://doi.org/10.1139/e75-161, 1975.

Kaufman, D. S., Jensen, B. J. L., Reyes, A. V., Schiff, C. J., Froese, D. G., and Pearce, N. J. G.: Late Quaternary tephrostratigraphy, Ahklun Mountains, SW Alaska, J. Quaternary Sci., 27, 344–359, https://doi.org/10.1002/jqs.1552, 2012.

Kaufman, D. S., Axford, Y. L., Henderson, A. C. G., McKay, N. P., Oswald, W. W., Saenger, C., Anderson, R. S., Bailey, H. L., Clegg, B., Gajewski, K., Hu, F. S., Jones, M. C., Massa, C., Routson, C. C., Werner, A., Wooller, M. J., and Yu, Z.: Holocene climate changes in eastern Beringia (NW North America) – A systematic review of multi-proxy evidence, Quaternary Sci. Rev., 147, 312–339, https://doi.org/10.1016/j.quascirev.2015.10.021, 2016.

Kennedy, K. E., Froese, D. G., Zazula, G. D., and Lauriol, B.: Last Glacial Maximum age for the northwest Laurentide maximum from the Eagle River spillway and delta complex, northern Yukon, Quaternary Sci. Rev., 29, 1288–1300, https://doi.org/10.1016/j.quascirev.2010.02.015, 2010.

Kuehn, S. C., Froese, D. G., and Shane, P. A. R.: The INTAV intercomparison of electron-beam microanalysis of glass by tephrochronology laboratories: Results and recommendations, Quatern. Int., 246, 19–47, https://doi.org/10.1016/j.quaint.2011.08.022, 2011.

Kyle, P. R., Ponomareva, V. V., and Rourke Schluep, R.: Geochemical characterization of marker tephra layers from major Holocene eruptions, Kamchatka Peninsula, Russia, Int. Geol. Rev., 53, 1059–1097, https://doi.org/10.1080/00206810903442162, 2011.

Lakeman, T. R., Clague, J. J., Menounos, B., Osborn, G. D., Jensen, B. J. L., and Froese, D. G.: Holocene tephras in lake cores from northern British Columbia, Canada, Can. J. Earth Sci., 45, 935–947, https://doi.org/10.1139/E08-035, 2008.

Lerbekmo, J. F.: The White River Ash: largest Holocene Plinian tephra, Can. J. Earth Sci., 45, 693–700, https://doi.org/10.1139/E08-023, 2008.

Litton, C. D. and Buck, C. E.: The Bayesian Approach To the Interpretation of Archaeological Data, Archaeometry, 37, 1–24, https://doi.org/10.1111/j.1475-4754.1995.tb00723.x, 1995.

Lowe, D. J., Pearce, N. J. G., Jorgensen, M. A., Kuehn, S. C., Tryon, C. A., and Hayward, C. L.: Correlating tephras and cryptotephras using glass compositional analyses and numerical and statistical methods: Review and evaluation, Quaternary Sci. Rev., 175, 1–44, https://doi.org/10.1016/j.quascirev.2017.08.003, 2017.

Lowe, J. J. and Walker, M. J. C.: Radiocarbon Dating the Last Glacial-Interglacial Transition (Ca. 14–9 $^{14}$C Ka Bp) in Terrestrial and Marine Records: The Need for New Quality Assurance Protocols, Radiocarbon, 42, 53–68, https://doi.org/10.1017/s0033822200053054, 2000.

Lund, S., Keigwin, L., and Darby, D.: Character of Holocene paleomagnetic secular variation in the tangent cylinder: Evidence from the Chukchi Sea, Phys. Earth Planet. In., 256, 49–58, https://doi.org/10.1016/j.pepi.2016.03.005, 2016.

Mackay, H., Hughes, P. D. M., Jensen, B. J. L., Langdon, P. G., Pyne-O'Donnell, S. D. F., Plunkett, G., Froese, D. G., Coulter, S. E., and Gardner, J. E.: A mid to late Holocene cryptotephra framework from eastern North America, Quaternary Sci. Rev., 132, 101–113, https://doi.org/10.1016/j.quascirev.2015.11.011, 2016.

Melekestsev, I. V., Felitsyn, S. B., and Kiryanov, V. Y.: The eruption of Opala in A. D. 500 – the largest explosive eruption in Kamchatka in the Christian era, J. Volcanol. Seismol., 13, 21–36, 1992.

Miller, T. P., McGimsey, R. G., Richter, D. H., Riehle, J. R., Nye, G. J., Yount, M. E., and Dumoulin, J. A.: Catalog of the historically active volcanoes of Alaska, U. S. Dept. of the Interior, U. S. Geological Survey, Open-File Report 98-0582, 104 pp., https://doi.org/10.3133/ofr98582, 1998.

Monteath, A. J., van Hardenbroek, M., Davies, L. J., Froese, D. G., Langdon, P. G., Xu, X., and Edwards, M. E.: Chronology and glass chemistry of tephra and cryptotephra horizons from lake sediments in northern Alaska, USA, Quaternary Res., 88, 169–178, https://doi.org/10.1017/qua.2017.38, 2017.

Moore, T. C., Rea, D. K., and Godsey, H.: Regional variation in modern radiocarbon ages and the hard-water effects in Lakes Michigan and Huron, J. Paleolimnol., 20, 347–351, https://doi.org/10.1023/A:1007920723163, 1998.

Neal, C. A., McGimsey, R. G., Miller, T. P., Riehle, J. R., and Waythomas, C. F.: Preliminary Volcano-Hazard Assessment for Aniakchak Volcano, Alaska, U.S. Geological Survey, Open-File Report 00-519, 42 pp., https://doi.org/10.3133/ofr00519, 2000.

Nelson, R. E., Carter, L. D., and Robinson, S. W.: Anomalous Radiocarbon Ages from a Holocene Detrital Organic Lens in Alaska and their Implications for Radiocarbon Dating and Paleoenvironmental Reconstructions in the Arctic, Quaternary Res., 29, 66–71, https://doi.org/10.1016/0033-5894(88)90072-5, 1988.

Nielsen, C. H. and Sigurdsson, H.: Quantitative methods for electron microprobe analysis of sodium in natural and synthetic glasses, Am. Mineral., 66, 547–552, 1981.

Ólafsdóttir, S., Geirsdóttir, Á., Miller, G. H., Stoner, J. S., and Channell, J. E. T.: Synchronizing holocene lacustrine and marine sediment records using paleomagnetic secular variation, Geology, 41, 535–538, https://doi.org/10.1130/G33946.1, 2013.

Oldfield, F., Thompson, R., Crooks, P. R. J., Gedye, S. J., Hall, V. A., Harkness, D. D., Housley, R. a., McCormac, F. G., Newton, A. J., Pilcher, J. R., Renberg, I., and Richardson, N.: Radiocarbon dating of a recent high latitude peat profile: Stor Åmyran, northern Sweden, Holocene, 7, 283–290, https://doi.org/10.1177/095968369700700304, 1997.

Olsson, I. U.: Some problems in connection with the evaluation of C 14 dates, Geol. Föreningen i Stock. Förhandlingar, 96, 311–320, https://doi.org/10.1080/11035897409454285, 1974.

Oswald, W. W., Anderson, P. M., Brown, T. A., Brubaker, L. B., Hu, F. S., Lozhkin, A. V., Tinner, W., and Kaltenrieder, P.: Effects of sample mass and macrofossil type on radiocarbon dating of arctic and boreal lake sediments, Holocene, 15, 758–767, https://doi.org/10.1191/0959683605hl849rr, 2005.

Payne, R. J. and Blackford, J. J.: Distal micro-tephra deposits in southeast Alaskan peatlands, Yukon Explor. Geol. 2003, 191–197, 2004.

Payne, R. J., Blackford, J., and van der Plicht, J.: Using cryptotephras to extend regional tephrochronologies: An example from southeast Alaska and implications for hazard assessment, Quaternary Res., 69, 42–55, https://doi.org/10.1016/j.yqres.2007.10.007, 2008.

Pearce, C., Varhelyi, A., Wastegård, S., Muschitiello, F., Barrientos, N., O'Regan, M., Cronin, T. M., Gemery, L., Semiletov, I., Backman, J., and Jakobsson, M.: The 3.6 ka Aniakchak tephra in the Arctic Ocean: a constraint on the Holocene radiocarbon reservoir age in the Chukchi Sea, Clim. Past, 13, 303–316, https://doi.org/10.5194/cp-13-303-2017, 2017.

Pearce, N. J. G., Westgate, J. A., Preece, S. J., Eastwood, W. J., and Perkins, W. T.: Identification of Aniakchak (Alaska) tephra in Greenland ice core challenges the 1645 BC date for Minoan eruption of Santorini, Geochem. Geophy. Geosy., 5, Q03005, https://doi.org/10.1029/2003GC000672, 2004.

Pilcher, J. R., Hall, V. A., and McCormac, F. G.: Dates of Holocene Icelandic volcanic eruptions from tephra layers in Irish peats, Holocene, 5, 103–110, https://doi.org/10.1177/095968369500500111, 1995.

Plunkett, G.: Tephra-linked peat humification records from Irish ombrotrophic bogs question nature of solar forcing at 850 cal yr BC, J. Quaternary Sci., 21, 9–16, https://doi.org/10.1002/jqs.951, 2006.

Plunkett, G., Coulter, S. E., Ponomareva, V. V., Blaauw, M., Klimaschewski, A., and Hammarlund, D.: Distal tephrochronology in volcanic regions: Challenges and insights from Kamchatkan lake sediments, Global Planet. Change, 134, 26–40, https://doi.org/10.1016/j.gloplacha.2015.04.006, 2015.

Ponomareva, V., Portnyagin, M., Pendea, I. F., Zelenin, E., Bourgeois, J., Pinegina, T., and Kozhurin, A.: A full holocene tephrochronology for the Kamchatsky Peninsula region: Applications from Kamchatka to North America, Quaternary Sci. Rev., 168, 101–122, https://doi.org/10.1016/j.quascirev.2017.04.031, 2017.

Ponomareva, V., Polyak, L., Portnyagin, M., Abbott, P. M., Zelenin, E., Vakhrameeva, P., and Garbe-Schönberg, D.: Holocene tephra from the Chukchi-Alaskan margin, Arctic Ocean: Implications for sediment chronostratigraphy and volcanic history, Quat. Geochronol., 45, 85–97, https://doi.org/10.1016/j.quageo.2017.11.001, 2018.

Portnyagin, M. V., Ponomareva, V. V., Zelenin, E. A., Bazanova, L. I., Pevzner, M. M., Plechova, A. A., Rogozin, A. N., and Garbe-Schönberg, D.: TephraKam: geochemical database of glass compositions in tephra and welded tuffs from the Kamchatka volcanic arc (northwestern Pacific), Earth Syst. Sci. Data, 12, 469–486, https://doi.org/10.5194/essd-12-469-2020, 2020.

Preece, S. J., McGimsey, R. G., Westgate, J. A., Pearce, N. J. G., Hart, W. K., and Perkins, W. T.: Chemical complexity and source of the White River Ash, Alaska and Yukon, Geosphere, 10, 1020–1042, https://doi.org/10.1130/GES00953.1, 2014.

Pyne-O'Donnell, S. D. F.: The taphonomy of Last Glacial-Interglacial Transition (LGIT) distal volcanic ash in small Scottish lakes, Boreas, 40, 131–145, https://doi.org/10.1111/j.1502-3885.2010.00154.x, 2010.

Pyne-O'Donnell, S. D. F., Hughes, P. D. M., Froese, D. G., Jensen, B. J. L., Kuehn, S. C., Mallon, G., Amesbury, M. J., Charman, D. J., Daley, T. J., Loader, N. J., Mauquoy, D., Street-Perrott, F. A., and Woodman-Ralph, J.: High-precision ultra-distal Holocene tephrochronology in North America, Quaternary Sci. Rev., 52, 6–11, https://doi.org/10.1016/j.quascirev.2012.07.024, 2012.

Reimer, P. J., Austin, W. E. N., Bard, E., Bayliss, A., Blackwell, P. G., Bronk Ramsey, C., Butzin, M., Cheng, H., Edwards, R. L., Friedrich, M., Grootes, P. M., Guilderson, T. P., Hajdas, I., Heaton, T. J., Hogg, A. G., Hughen, K. A., Kromer, B., Manning, S. W., Muscheler, R., Palmer, J. G., Pearson, C., van der Plicht, J., Reimer, R. W., Richards, D. A., Scott, E. M., Southon, J. R., Turney, C. S. M., Wacker, L., Adolphi, F., Büntgen, U., Capano, M., Fahrni, S. M., Fogtmann-Schulz, A., Friedrich, R., Köhler, P., Kudsk, S., Miyake, F., Olsen, J., Reinig, F., Sakamoto, M., Sookdeo, A., and Talamo, S.: The IntCal20 Northern Hemisphere Radiocarbon Age Calibration Curve (0–55 cal kBP), Radiocarbon, 62, 725–757, https://doi.org/10.1017/RDC.2020.41, 2020.

Reuther, J., Potter, B., Coffman, S., Smith, H., and Bigelow, N.: Revisiting the Timing of the Northern Lobe of the White River Ash Volcanic Event in Eastern Alaska and Western Yukon, Radiocarbon, 62, 169–188, https://doi.org/10.1017/RDC.2019.110, 2020.

Riehle, J. R., Meyer, C. E., Ager, T. A., Kaufman, D. S., and Ackerman, R. E.: The Aniachak tephra deposit, a late Holocene marker horizon in western Alaska, in: Geologic studies in Alaska by the U.S. Geological Survey during 1986, edited by: Hamilton, T. D. and Galloway, J. P., U.S. Geological Survey Circular 998, 19–23, https://dggs.alaska.gov/pubs/id/26602 (last access: 23 February 2022), 1987.

Saxby, J., Rust, A., Cashman, K., and Beckett, F.: The importance of grain size and shape in controlling the dispersion of the Vedde cryptotephra, J. Quaternary Sci., 35, 175–185, https://doi.org/10.1002/jqs.3152, 2020.

Schoning, K., Charman, D. J., and Wastegård, S.: Reconstructed water tables from two ombrotrophic mires in eastern central Sweden compared with instrumental meteorological data, Holocene, 15, 111–118, https://doi.org/10.1191/0959683605hl772rp, 2005.

Schuur, E. A. G., Bockheim, J., Canadell, J. G., Euskirchen, E., Field, C. B., Goryachkin, S. V., Hagemann, S., Kuhry, P., Lafleur, P. M., Lee, H., Mazhitova, G., Nelson, F. E., Rinke, A., Romanovsky, V. E., Shiklomanov, N., Tarnocai, C., Venevsky, S., Vogel, J. G., and Zimov, S. A.: Vulnerability of Permafrost Carbon to Climate Change: Implications for the Global Carbon Cycle, Bioscience, 58, 701–714, https://doi.org/10.1641/B580807, 2008.

Steen, D. P.: Late Quaternary Paleomagnetism and Environmental Magnetism at Cascade and Shainin Lakes, North-Central Brooks Range, Alaska, Northern Arizona University, thesis, ProQuest Number: 10126253, https://www.proquest.com/docview/1808501293 (last access: 23 February 2022), 2016.

Stelling, P., Gardner, J. E., and Begét, J.: Eruptive history of Fisher Caldera, Alaska, USA, J. Volcanol. Geoth. Res., 139, 163–183, https://doi.org/10.1016/j.jvolgeores.2004.08.006, 2005.

Stevenson, J. A., Millington, S. C., Beckett, F. M., Swindles, G. T., and Thordarson, T.: Big grains go far: understanding the discrepancy between tephrochronology and satellite infrared measurements of volcanic ash, Atmos. Meas. Tech., 8, 2069–2091, https://doi.org/10.5194/amt-8-2069-2015, 2015.

Stoner, J. S., Channell, J. E. T., Mazaud, A., Strano, S. E., and Xuan, C.: The influence of high-latitude flux lobes on the Holocene paleomagnetic record of IODP Site U1305 and the northern North Atlantic, Geochem. Geophy. Geosy., 14, 4623–4646, https://doi.org/10.1002/ggge.20272, 2013.

Swindles, G. T., De Vleeschouwer, F., and Plunkett, G.: Dating peat profiles using tephra: stratigraphy, geochemistry and chronology, Mires Peat, 7, 1–9, 2010.

Turney, C. S. M., Coope, G. R., Harkness, D. D., Lowe, J. J., and Walker, M. J. C.: Implications for the Dating of Wisconsinan (Weichselian) Late-Glacial Events of Systematic Radiocarbon Age Differences between Terrestrial Plant Macrofossils from a Site in SW Ireland, Quaternary Res., 53, 114–121, https://doi.org/10.1006/qres.1999.2087, 2000.

Tylmann, W., Bonk, A., Goslar, T., Wulf, S., and Grosjean, M.: Calibrating 210Pb dating results with varve chronology and independent chronostratigraphic markers: Problems and implications, Quat. Geochronol., 32, 1–10, https://doi.org/10.1016/j.quageo.2015.11.004, 2016.

van der Bilt, W. G. M., Lane, C. S., and Bakke, J.: Ultra-distal Kamchatkan ash on Arctic Svalbard: Towards hemispheric cryptotephra correlation, Quaternary Sci. Rev., 164, 230–235, https://doi.org/10.1016/j.quascirev.2017.04.007, 2017.

Vinther, B. M., Clausen, H. B., Johnsen, S. J., Rasmussen, S. O., Andersen, K. K., Buchardt, S. L., Dahl-Jensen, D., Seierstad, I. K., Siggaard-Andersen, M. L., Steffensen, J. P., Svensson, A., Olsen, J., and Heinemeier, J.: A synchronized dating of three Greenland ice cores throughout the Holocene, J. Geophys. Res., 111, D13102, https://doi.org/10.1029/2005JD006921, 2006.

Waitt, R. B. and Begét, J. E.: Volcanic processes and geology of Augustine Volcano, Alaska: U.S. Geological Survey Professional Paper 1762, 2 plates, scale 1:25,000, 79 pp., https://doi.org/10.3133/pp1762, 2009.

Wallace, K. L., Hayden, L. A., and Neal, C. A.: Major-element glass compositions of tephra from the circa 3.6 ka eruption of Aniakchak volcano, Alaska Peninsula, Alaska, Alaska Division of Geological & Geophysical Surveys [data set], Raw Data File 2017-9, 9 p., https://doi.org/10.14509/29777, 2017.

Watson, E. J., Swindles, G. T., Lawson, I. T., and Savov, I.: Spatial variability of tephra and carbon accumulation in a Holocene peatland, Quaternary Sci. Rev., 124, 248–264, https://doi.org/10.1016/j.quascirev.2015.07.025, 2015.

Watt, S. F. L., Gilbert, J. S., Folch, A., Phillips, J. C., and Cai, X. M.: An example of enhanced tephra deposition driven by topographically induced atmospheric turbulence, B. Volcanol., 77, 35, https://doi.org/10.1007/s00445-015-0927-x, 2015.

Zander, P. D., Kaufman, D. S., Mckay, N. P., Kuehn, S. C., and Henderson, A. C. G.: Quaternary Geochronology Using correlated tephras to re fi ne radiocarbon-based age models, upper and lower Whitshed Lakes, south-central Alaska, Quat. Geochronol., 45, 9–22, https://doi.org/10.1016/j.quageo.2018.01.005, 2018.

Zoltai, S. C.: Late Quaternary volcanic ash in the peatlands of central Alberta, Can. J. Earth Sci., 26, 207–214, https://doi.org/10.1139/e89-017, 1989.